5-2007

Design and Development of an in-house Scanning Tunneling Microscope System

Esvar Subramanian
Clemson University, esubram@clemson.edu

DESIGN AND DEVELOPMENT OF AN IN-HOUSE SCANNING TUNNELING MICROSCOPE SYSTEM

A Thesis
Presented to
the Graduate School of
Clemson University

In Partial Fulfillment
of the Requirements for the Degree
Master of Science
Mechanical Engineering

---

by
Esvar Chandran Subramanian
May 2007

Accepted by:
Dr.Nader Jalili, Committee Chair
Dr.Chad Sosolik
Dr.Darren Dawson

ABSTRACT

The invention of Scanning Tunneling Microscope (STM) by Binnig and Rohrer in 1982 eliminated the use of optical lenses and replaced the conventional optical microscopes with a new class of microscopes called the Scanning Probe Microscopes (SPM). Because of their unique characteristics such as higher resolution and acquisition of nano level images without affecting the physical properties of the sample, they have found wide applications in a variety of scientific disciplines such as biology, material science and electrochemistry. After considerable advancements in instrumentation, the STM has evolved as a nanomanipulation and nanofabrication tool. It operates in two modes: constant current mode and constant height mode. In constant current mode, the feedback parameter is the tunneling current based on which the voltage applied to the piezoelectric actuator is varied. Hence, the tip height is varied in accordance with this tunneling current. In the constant height mode, however, the height is maintained at a constant value and hence the voltage applied to the piezoelectric actuator is adjusted (PZT). Unlike constant current mode, it is the tunneling current which changes according to the surface profile and the local electronic structure of the tip and the sample.

The present research is an effort in designing and fabricating an in-house STM to be operated in the constant current mode by interfacing various subsystems. The various subsystems constituting the experimental setup mainly include a micro positioner, a nano stager, STM Electronics, and STM head. The fabrication process involved testing and verification of a suitable preamplifier for providing the feedback signal, design of the STM head and development of a computer automated system in order to facilitate the acquisition of signals related to a micro positioner which acts as the coarse positioner. The software control consists of ControlDesk® as the front end and Simulink® as the backend. An optical subsystem in the form of a high resolution camera that has been interfaced facilitates visual monitoring and development of dual stage control of the fine as well as coarse positioners. The ability of the STM to acquire images at the nano level is attributed to the tip to sample interaction based on quantum mechanical tunneling. To better understand the aspects of STM, the present work also traces the development of theoretical modeling of the tip-sample interaction and the conceptual design of other classes of microscopes belonging to the SPM family. Certain hardware limitations associated with the data acquisition board need to be addressed in order to acquire nanolevel images. The future scope of the research would include development and testing of various types of controllers on the STM test bed.

DEDICATION

This thesis is dedicated to my family, teachers and friends.

ACKNOWLEDGEMENTS

At the outset I would like to thank my parents for having encouraged me to pursue higher education.

I'm gratefully indebted to my advisor Dr. Nader Jalili, who gave me an opportunity to carry out research under his tutelage. His guidance, support and above all infinite patience with me proved to be a constant source of inspiration throughout the research project. I would also like to thank my committee member Dr. Chad Sosolik from Department of Physics and Astronomy, Clemson University, who gave me an opportunity to practically see and learn the operation of STM in his lab. I would also like to express my sincere thanks on an equal basis to my other committee member Dr. Darren Dawson from the Department of Electrical and Computer Engineering, Clemson University, for monitoring the progress of my research work at frequent intervals.

I would also want to express my special thanks to Mr. Saeid Bashash, PhD student at the SSNEMS lab, Department of Mechanical Engineering, Clemson University. The discussions with him regarding the project always proved to be a source of guidance.

I would also like to specially thank Mr. David Moline, Department of Mechanical Engineering, Clemson University, who helped me in the electrical interfacing of the micro positioner with the existing research setup in the lab. I would also like to acknowledge Mr. Michael Justice, technician assistant in Department of Mechanical Engineering and personnel at the Precision Manufacturing Center, Clemson University for helping me to fabricate the various components of the test bed.

I would also want to thank Mr. Randy Emert from the Department of General Engineering, Clemson University for giving me access to the rapid prototyping machine thereby providing me an opportunity to experiment with various STM tip and sample models. Finally, I would like to thank all my present labmates: Nima Mahmoodi, Saeid Bashash, Reza Saeidpourazar, Reza Housseini, Mana Afshari, Amin Salehi, Sudeep Chavare and Prakash Venkataraman. I would also like to acknowledge the past members of SSNEMS lab: Miheer Gurjar, Vikrant Bhadbhade, Sandeep Hiremath, Virgile Ayglon and Himanshu Rajoria. Each of them acted as a source of support and inspiration in their own ways. I would also want to thank my room mates and friends at Clemson University whose association I would cherish for the years to come.

My sincere gratitude to all those people whom I may have forgotten to mention but have rendered help in their own ways.

TABLE OF CONTENTS

Page

.

Table of Contents (Continued)

Page

LIST OF FIGURES

List of Figures (Continued)

Figure Page

List of Figures (Continued)

Figure Page

NOMENCLATURE

a	width of the potential barrier
B_{sample}	Magnetic field emanating from the sample surface
$C(z)$	tip-surface capacitance
d	distance resolved between two point light sources
D_t	Density of states per unit volume of the probe tip
E	energy of the electron
E_μ	Energy of the state ψ_μ in the absence of tunneling
$f(E)$	Fermi Function
$F(z)$	Interaction between the tip and the sample
$\lvert f \rangle$	A current carrying state in the sample metal
$\hbar$	Reduced Planck's constant
h	height of the potential barrier
H^o	Hamiltonian of a 2 electrode system (capacitor) without tip atom
i	Momentum of the incoming electron
$<i+>$	wave with plane components propagating from the interior of the tip of the electrode towards the tunnel junction
J	current density
$M_{\mu\nu}$	Tunneling matrix
m	Magnetic dipole of the tip

m_e Mass of an electron

NA Numerical Aperture

P Probability density function for typical (rectangular) barrier penetration

V Potential in the barrier

$\Delta V = V_{tip} - V_{surf}$ the potential difference between the tip and the surface

V^{cap} Potential of the capacitor which includes the two electrodes

V^{tip} The potential induced by a tip atom, which would break any spatial symmetry that might exists for the two electrode system

z vertical tip-surface separation

Ψ_μ Tip wave function

Ψ_v Surface wave function

λ Wavelength of light used

α Angle of aperture

ω Voltage modulation frequency

δ_{AA}^{tip} The projection of the local function $|A\rangle$

δ_{AA}^{cap} Capacitor projected local density (CAP-LOD)

$\gamma(E)$ Transition conductivity at the tunneling energy E

σ Tunneling conductance

$\Psi(i)$ The initial state occupied by the electron

$\Psi(f)$ The final state occupied by the electron.

CHAPTER 1

INTRODUCTION

Evolution of Scanning Probe Microscopes from Optical Microscopes

It can be rightly said that the invention of magnifying glass marked the genesis of modern microscopy techniques. The conventional optical microscope was invented by Robert Hooke in the late 17th century [1]. The principle of obtaining images through a conventional optical microscope is focusing through a set of optical lenses [1]. The limitation in using the optical lenses is due to two factors which are angle of aperture and the wavelength of light [1]. The distance traveled between two point light sources is related to the wavelength as

$$d = 0.61\lambda / \sin\alpha \qquad (1.1)$$

Where λ corresponds to the wavelength of light used, α refers to the angle of aperture and d is the distance that can be resolved between two point light sources [1]. The shortest wavelength of light used is 400 nm hence this puts a ceiling of theoretical resolution obtainable by the optical microscopes to 200 nm [1, 2]. For obtaining images with an atomic resolution a shorter wavelength is required.

The formulation of hypothesis of quantum mechanics in the 1900s by theoretical physicists like Max Planck (and also the de-Broglie's attribution of wave and particle nature to matter) and the subsequent experimental verification of wave nature of electron by C.J. Davison and L.H. Germer in 1927 [1] wherein it was found that "a high energy electron has a shorter wavelength than a low energy electron" [1] paved the way for rapid progress in the field of electron microscope research.

The first electron microscope was invented by E. Ruska and M. Knoll in 1931 [1]. The electron microscopes use the electron rays instead of the light rays in order to focus by means of electrical coils [1]. “The magnifying power is greatly improved since the wavelength of these particles is much less than that of the light” [1]. The inadequacy of the electron microscope to acquire images at the atomic level is amply revealed by the following statement of Richard Feynman in the year 1959 [3]: “The electron microscope is not quite good enough, with the greatest care and effort it can only resolve about 10 angstroms…. Is there no way to make electron microscope more powerful?”[4]. Using electron microscopes a theoretical resolution of 4 nm was achieved but a still shorter wavelength was required in order to acquire atomic images. This was because of the fact that both “λ“and “d” in Equation (1.1) are of the same dimensions [1]. Hence from this condition we can infer that if atomic resolution images are to be obtained then the wavelength of light used should also be in the order of angstroms. X-rays and gamma rays are the electromagnetic radiations with wavelengths corresponding to that order of magnitude and the difficulty with the above electromagnetic radiations are that they cannot be focused by optical lenses [1]. The invention of Scanning Tunneling Microscope (STM) by Binnig and Rohrer in 1982 eliminated the use of optical lenses and replaced the conventional optical microscopes with a new class of microscopes called the Scanning Probe Microscopes (SPM) [1].

The invention of Atomic Force Microscope (AFM) in 1986 by Gerd Binnig satisfied the purpose of imaging insulating materials since the STM that was invented four years ago could acquire only images that were conducting [1]. In the initial stages the AFM differed from the STM in the sense that in the AFM the tip and the sample were in contact with

each other and the vander waals forces provided the contrast mechanism in the place of tunneling current as in STM [1]. An overview about the evolution of SPM can be found in [1]. The different classes of SPM and the description of each of them can be found in Chapter 2.

Applications of Scanning Probe Microscopy

"The objective of nanoscience and nanotechnology is to study, create or apply materials, devices and systems that could control matter at nanometric or even atomic dimension [5]". The ability of SPM to reach at the atomic level without affecting the biological or physical characteristics of the sample has helped in achieving the above objective. Thus owing to their versatility, the SPMs have tremendously affected various scientific disciplines; a short description about which is stated in the following lines.

Applications in Biology

In the year 1959, Richard Feynman in his lecture titled [3]," There is plenty of room at the bottom", noted "It is very easy to answer many of these fundamental biological questions; you just look at the thing! You will see the structure of the microsome. Unfortunately the present microscope sees at a level which is just a bit too crude. Make the microscope a hundred times more powerful, and many problems of biology would be made very much easier. " The invention of SPMs was a stepping stone in that direction of solving the problems of imaging in the field of biology as foreseen by Feynman.

Conventional microscopes like Scanning Electron Microscope, Transmission Electron Microscope and the Field Ion Microscope require the operating environment to be a vacuum environment [2]. Diffraction techniques are limited to crystalline samples and cannot provide local structural information in real space [2]. The above constraints

related to other microscopy techniques helped in the widespread application of SPM to biology. The biological samples under consideration loose their biological and physical properties when subjected to an environment other than their natural environment. SPMs remove all constraints like temperature conditions and environment conditions related to image acquisition owing to their versatility [2]. The early usage of STM in the field of biology was in the acquisition of images of an unstained DNA. Study of Nucleic acids: De-oxy-ribo-Nucleic Acid and Ribo-Nucleic Acid is made possible by AFM and STM (SPMs in general) in their natural conditions [2]. The images of DNA in aqueous solution obtained by AFM were first reported by Lindsay et.al in March 1988 [2, 6]. In the initial stages STM was used for imaging but with the invention of AFM by Gerd Binnig in 1986 [1, 7] the way was paved for imaging of insulation surfaces and biological specimens. Two years after the invention of STM in the year 1986, its inventors Binnig and Rohrer reported the image of a double helix [6, 8]. With advancement in instrumentation, the STMs ability was enhanced to acquire images in water [8, 9 and 10]. The advantages of the operation of STM in water are [8] "

- The hydration of the structure is maintained. Although this may limit resolution (because of the softer structure) it should allow more realistic imaging, particularly of biological process [11].
- The interface is far better controlled when in contact with a fluid, and, in principle, electrochemical methods permit control of depositions to within small fractions of a monolayer [12]. We can routinely obtain high resolution images without the need to hunt over a surface".

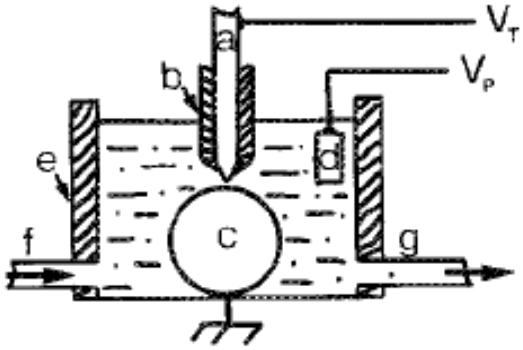

Figure 1.1: The schematic of the SPM electrochemistry cell used to image DNA samples in aqueous medium. (a) Pt tip (b) glass insulation (c) gold ball with flat facets (d) gold plating electrode (e) glass walls (f) inlet tube and (g) outlet tube [8].

Applications in Chemistry

"The STM due to its ability to image at the atomic level on $(\mu m)^2$ areas is well suited to investigate the relationship between surface morphology and the atomic mechanisms that determine it [13]". "The STM has provided an important new tool for both in situ and ex-situ characterization of electrodes. i.e., the imaging of surface structures at a scale ranging from submicron to atomic resolution and the acquisition of information about the electronic properties of the surface." [14]. Short range order and long range periodicity present in the structure of surfaces as well as disordered surface layers can easily be identified by STM. The electrochemical STM as shown in Figure 1.1 was first constructed by Sonnenfeld and Hansma to be operated under solution [7, 10]. There are widespread applications of SPM in the field of chemistry and in particular to electrochemistry. After the experimental demonstration of the ability of the STM to operate in an aqueous medium, the electrochemical STM was used to image the

electrochemical phenomena with an atomic or molecular resolution in real space. The STM is used as an investigative tool to study various processes related to electrochemistry such as “electro deposition of metals, corrosion, adsorption of species from solution, and changes in the structure of the electrode surface caused by the passage of current [14]”. The tunneling current which acts as the feedback signal contains important information about the electrochemical processes taking place between the tip and the sample. “It also contains valuable information about the electronic states of adsorbed molecules which could be used not only to identify the molecules but also to study the reactivity of the molecules [15]”. The process of adsorption of the small molecules on clean surfaces is particularly useful in the study of surface science owing to the applications to catalysis, corrosion and etching [2]. “After STM had demonstrated atomic resolution on semiconductor and metal surfaces, both with and without atomic adsorbates, it soon became a challenge to image molecules at surfaces and interfaces as well [2]”. In its developmental stages the issues related to acquiring images of molecular adsorbates had been attributed to rapid surface diffusion [2]. This process of surface diffusion is enhanced and aided by electric fields [2]. The reason for the difficulty in acquiring images of molecular adsorbates can also be due to the absence of molecular orbital near the fermi level [2]. After the issue of acquiring the STM images at the molecular surfaces and interfaces had been resolved the STM was widely used in providing information about the molecular properties and the molecule-surface interactions [2].

Applications in Material science

"In semi- conductor technology sub-micrometer features on integrated circuit boards can be measured to perform routine product information of failure analysis" [1]. In conjunction with techniques like secondary mass spectrometry and auger spectroscopy SPM evolved into a powerful technique to characterize thin film growth in molecular beam epitaxy [16]. STM is used to study various types of structures like polymers and ceramics. "The technique is suitable for determining surface structures such as porosity, fractures, defects, grain size, boundaries and distribution" [1].

Applications as a Nanofabrication Tool

"The STM, initially invented to image surfaces down to the atomic scale, has been further developed in the last few years to an operative tool, with which atoms and molecules can be manipulated at will at low substrate temperatures in different manners to create and investigate artificial structures whose properties can be investigated employing spectroscopic dI/dV measurements [17]". The ability of the STM to obtain highly spatial resolution images is due to the close proximity of the tip to the sample as to make the electron current highly spatially confined [2]. The tip of the STM is the component that plays a major role in nanofabrication. "The small distance between the tip and the sample, which is about one nanometer, causes electrons to tunnel to (or from) a region on the sample that is approximately one nanometer in diameter, with an even smaller major distribution area. Thus, the surface fabrication produced by STM must be performed on the nanometer scale .i.e., STM can nanofabricate" [2].

The advantage of using STM in the surface fabrication process is that it plays a multi purpose role [2]:

a) It can detect the defects in masks and circuits.
b) Repair them by surface deposition and etching.
c) Finally examine the results by (STM) itself.

The STM can be used to manipulate atoms or clusters at will by modifying the growth, migration and diffusion of clusters on surfaces, controlling and performing the interactions between particles and substrates as well as interactions between small particles [2].

Thesis Contributions

The present work is directed towards designing, developing and integrating various sub systems in order to fabricate and build an in-house scanning tunneling microscope.

The STM that has been fabricated consists of:

a) Coarse positioner (in the form of a micro positioner)
b) Fine positioner (in the form of a nano stager)
c) Optical subsystem (which facilitates in the dual control of the fine as well as the coarse positioner)
d) STM Head (which constitutes tip holder and sample holder)
e) STM Electronics- A preamplifier circuit that provides the feedback signal
f) dSPACE® DS1104 R& D controller board-to control the micro-positioner
g) C-809 Motion I/O® controller -An auxiliary apparatus for controlling the PZT

The STM thus built by integrating the above sub systems acts as a test bed. In this test bed the effectiveness of various types of controllers for coarse and fine positioning could be tested. The creation of the test bed also involved automation using software (Simulink® in the back end and ControlDesk® in the front end). This software control was established to facilitate the operation and control of the micro-positioner and the STM as a whole. For a better insight into the aspects of Scanning Probe Microscopy the work also covers an elaborate literature survey involving the historical evolution of SPM, an overview of different types of scanning probes microscopes and a mathematical modeling dealing with the tip to sample interaction.

Thesis Outline

Chapter 1 deals with the introduction and the general applications of SPM. Chapter 2 covers the different types under the family of SPMs. Chapter 3 attempts to discuss about the different theoretical models of tip to sample interaction. Chapter 4 describes various subsystems that constitute the experimental set up. Chapter 5 discusses the results that were obtained pertaining to the micropositioner and the preamplifier. The thesis is concluded with chapter 6 where future scope of the project is dealt with.

Chapter Summary

This gave an overview about the evolution of Scanning Probe Microscopy from Optical Microscopes. It also discusses about the widespread applications of SPM in different scientific disciplines ranging from chemistry to biology.

CHAPTER 2

CONCEPTUAL DESIGN AND OPERATION OF A SCANNING PROBE MICROSCOPE

Introduction

SPMs refer to a general family of microscopes. The principle of operation of which is based on the interaction of the tip and sample in order to observe the physical properties of the sample like spectroscopic and structural properties on an atomic scale. Scanning Probe Microscopy technique provides three-dimensional real space images and among surface analysis techniques, it allows spatially localized measurements of structure and properties [14]. The surface image of the sample is reconstructed by moving the scanner, line by line over the sample. In a SPM the tip doesn't touch the sample. Hence, the scanner is also required to maintain an optimum distance that is constrained by the interaction. The distance between the tip and the sample is in the order of sub-angstrom units. Depending upon the modes of "interaction" the general class of Scanning Probe Microscopy is classified as:

a) Scanning Tunneling Microscopy (STM)
b) Atomic Force Microscopy (AFM)
c) Magnetic Force Microscopy (MFM)
d) Lateral force Microcopy (LFM)
e) Force Modulation Microscopy (FMM)
f) Phase detection Microscopy (PMM)
g) Electrostatic Force Microscopy (EFM)

h) Scanning Capacitance Microscopy (SCM)

i) Scanning Thermal Microscopy (SThM)

j) Near field Scanning Optical Microscopy (NSOM)

Brief Overview of Various Types of SPM s

Scanning Tunneling Microscope

STM was the original class of Scanning Probe Microscope that was invented by Gerd Binnig and Heinrich Rohrer at IBM Zurich in 1981, for which they were awarded the Nobel Prize in Physics in 1986. In a STM, a voltage bias is applied between the tip (which is a sharp conducting one) and the sample, and when the tip is brought close to the sample depending on the sign of the bias voltage the tunneling phenomena takes place either from the tip to the sample or vice versa. The tunneling current which is the feedback signal for acquiring images at the nano level is a negative exponential function of the sample surface and the STM tip. It is this exponential characteristic that gives the STM its high sensitivity and was the reason for the shift of focus of research from conventional optical microscopes to the Scanning Probe Microscopes and marked the genesis of the class of SPM s [2]. Conventional optical microscopes are limited by the value of the wavelength of the visible light which is $0.4\mu m$. So this inherent limitation of the optical microscopes limits their usage. Hence this necessitated the advent of STMs for obtaining three dimensional, real space images of surfaces with high spatial resolution [14]. The STMs operate based on the principle of quantum mechanical tunneling, about which has been dealt in the later chapters under the title of Theoretical Modeling of Scanning Tunneling Microscopy.

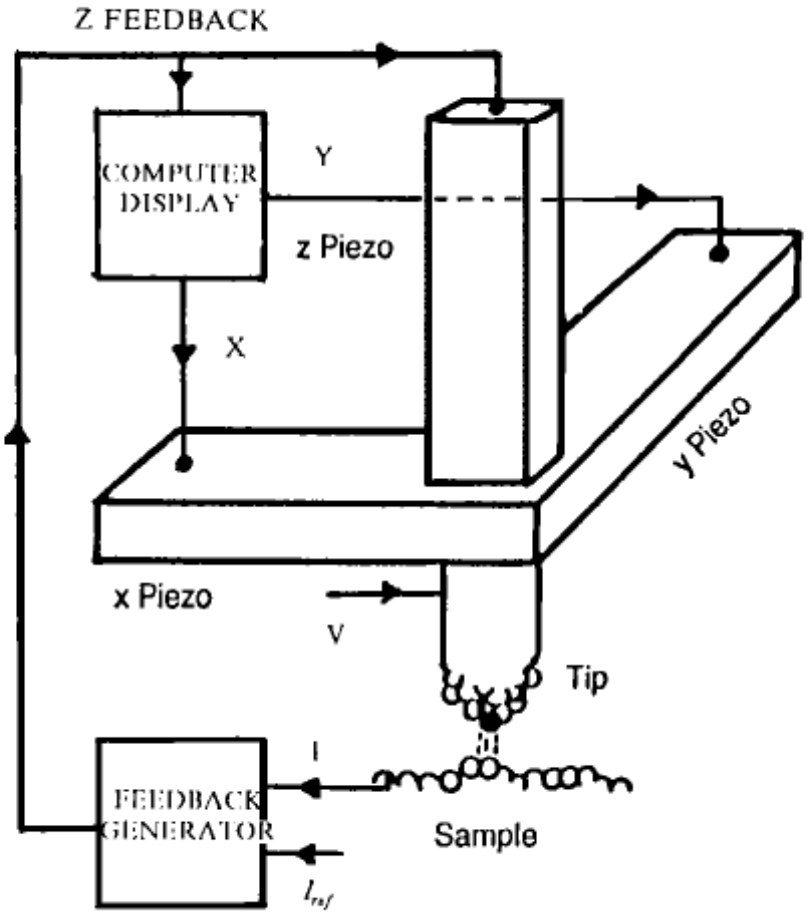

Figure 2.1: Schematic of a Scanning Tunneling Microscope [18].

The STM operates in two different modes: constant-height mode and constant current mode.

Constant Current Mode

In constant current mode as the name, suggests the tunneling current between the tip and the sample is maintained at a constant value. The feedback parameter is the tunneling current based on which the voltage applied to the piezoelectric transducer is varied. So the tip height (i.e. in the Z direction) is varied in accordance with this tunneling current. When it is sensed after feed back that the tunneling current is small; the tip to sample height is increased in order to maintain a preset value. So the variation of the feedback voltage applied in the Z direction is the image of the sample and represents a constant charge density contour of the surface [14].

Constant Height Mode

In the constant height mode, the height is maintained at a constant value and hence the voltage applied to the Piezoelectric Transducer (PZT). But it is the tunneling current which changes according to the surface profile and the local electronic structure of the tip and the sample. Hence in this mode, the tunneling current contains data about the surface profile of the sample and in turn is related to the charge density [14].The disadvantages and the advantages of the two modes are: In the constant height mode the scanning is faster because it is not limited by the response time of the Z scanner [14]. But the corrugations and variations in the surface profile cannot be traced in the constant height mode. In the constant current mode the surface irregularities are traced and the scanning time is comparatively higher.

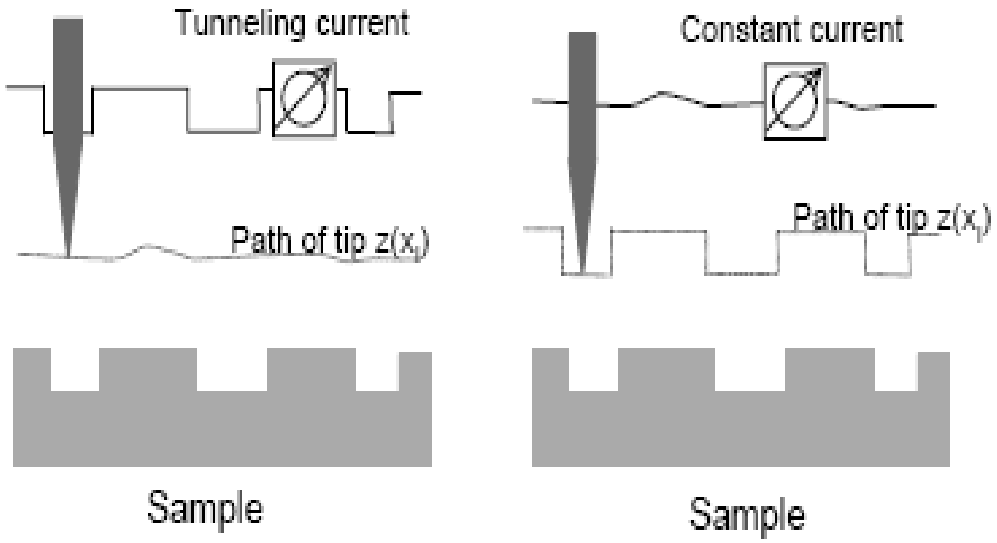

Constant height mode Constant current mode

Figure 2.2: Operation of Scanning Tunneling Microscope in both Constant height as well as Constant current mode. [19].

Atomic Force Microscope

The atomic force microscope has a tip attached to the free end of a cantilever probe. The interactions between the tip and the sample affect the deflections of the cantilever. The cantilever deflections are used to image the topography of the sample. ”Keeping the deflection constant and by varying the vertical position of the tip produces a constant force image analogous to the constant current STM” [14]. This displays the changes in surface height during scanning. This mode also gives calibrated height display about the sample surface [23]. The deflections in the cantilever probe acts as the feedback signal to correct the height so this mode is called as the error-Signal mode [20, 21]. When there is a profile change during the raster scanning of the sample then the amplitude of oscillation of the cantilever also correspondingly changes.

The objective of the feedback loop in that case will be to keep the amplitude of the oscillation of the cantilever constant [22]. Hence with this objective arise three open loop modes which are: non-contact mode AFM or attractive AFM, contact mode AFM or repulsive AFM, and tapping mode AFM.

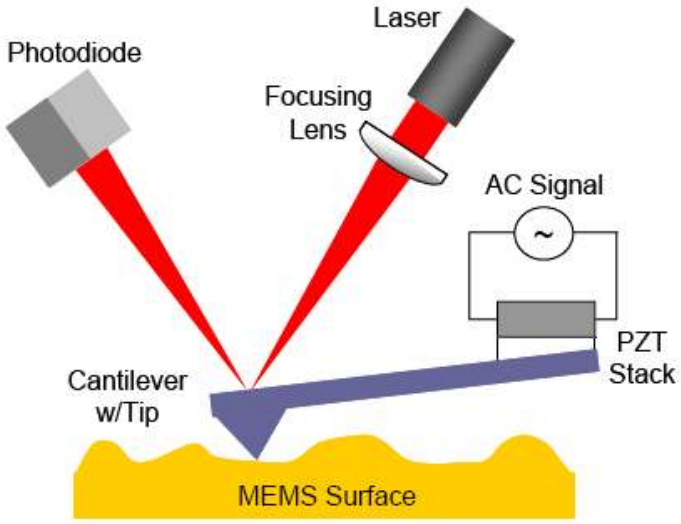

Figure 2.3 Diagram of an Atomic Force Microscope System [23]

Various modes of operation of the AFM are given in Table 2.1 [24]

Table 2.1: Lists of various modes of operation of AFM [24]

Mode of Operation	Force of Interaction
Contact Mode	Strong (repulsive) –constant force or constant distance
Non –contact mode	Weak (attractive) – vibrating mode
Intermittent contact mode	Strong (repulsive) –vibrating mode
Lateral Force mode	Frictional forces exert a torque on the scanning cantilever
Magnetic Force	The magnetic field of the surface is imaged
Thermal Scanning	The distribution of thermal conductivity is imaged.

Contact AFM or the Repulsive AFM

The AFM tip maintains a slight "contact or touch" with the sample surface. The spring constant of the cantilever beam which holds the tip is lower than the spring constant of the atoms of the sample that are held together [18, 22]. "The contact mode acquires sample attributes by monitoring interaction forces while the cantilever tip remains in contact with the target sample [18, 25]". An understanding about the interaction of the tip and the sample can be got from the analysis of van der Waals Force curve: From Figure 2.4, we can observe that initially the distance between the tip and the sample is large. The atom at the tip of the AFM and the atom on the sample, when are slowly brought close to each other, then there exists a weak force of attraction between them. There is also a

counter acting electrostatic force of repulsion existing between the electron clouds and this force of repulsion is predominant when the atomic distance between the tip of the atom and the sample decreases. The repulsive force counteracts the attractive force between the tip and the sample. This is attributed to decrease in inter atomic distance. The force becomes fully repulsive when the distance between the tip and the sample is only a few angstroms. "In AFM this means that when the cantilever pushes the tip against the sample, the cantilever bends rather than forcing the tip atoms closer to the sample atoms" [18]. The disadvantage of the probe tip remaining in contact with the sample is that the sample gets damaged as there are lateral dragging forces exerted by the probe tip.

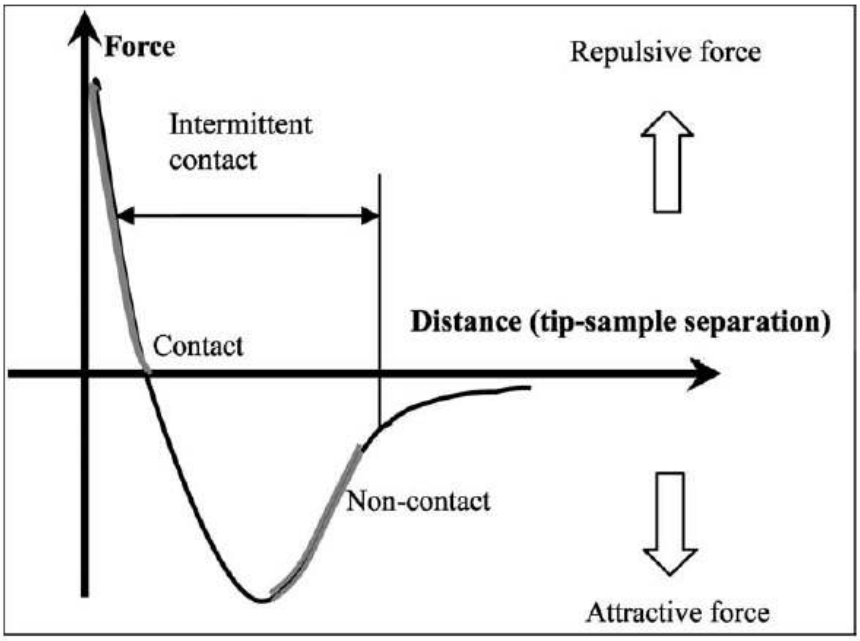

Figure 2.4: Inter-atomic force variation versus distance between AFM tip and sample [22].

Apart from the above mentioned repulsive forces, there are also present capillary forces which are attributed to the presence of a contaminant layer (which is in the form of a thin water layer) over the sample surface and the force exerted by the cantilever beam itself. The capillary force existing between the sample and the tip can be approximated to that of a force of a compressed spring [18]. Assuming the distance between the tip and the sample is incompressible and also the water layer is homogenous the magnitude of the capillary force between the tip and the sample is constant. However, the magnitude and the sign (repulsive or attractive) of the cantilever depend on the deflection and the spring constant of the cantilever [18, 22].The two modes of operation in a Contact AFM are: constant height mode and constant force mode. In the constant height mode the sample is scanned laterally and the z height between the tip and the sample is constant [18, 22]. Hence the deflection of the cantilever is used to obtain the surface profile of the sample. The drawback of this technique is that there is a high probability of the tip getting damaged when it may encounter a mountain or steep steps on the sample surface, as it is constantly in "Contact" with the sample surface during the scanning process [18, 22].

Constant Force Method

This is the most common mode in which the AFM is operated [18, 22]. A feedback loop is incorporated which maintains the height between the tip and the sample as constant. In constant force mode the deflection of the cantilever is used as the input to the feedback circuit so that the z-height is adjusted in accordance with the variations in the surface profile [18, 22]. So the voltage applied to the PZT is in such a way that it lowers or raises the cantilever to maintain the preset deflection value and thus maintains a constant force between the tip and the sample. This value of the voltage applied to the PZT by the

feedback system gives the surface profile of the sample under scan [18, 22]. In constant force mode since a feedback loop is involved, the time to scan a given area of the sample is large. The force applied on the sample by the tip is controlled [18]. Constant-height mode is more preferred for atomically flat surfaces because of the above mentioned disadvantage of the tip getting damaged.

In general, the contact AFM has the following features [24]:

- 3-D images at the nano level are obtained without damaging the sample.
- Sample treatment and preparation is comparatively minimal.
- Existence of repulsive force between the tip and the sample.
- Useful in analyzing insulators and conductors easily, as it is not based on conductivity contrary to STM.
- Capable of operation in both air as well as fluid environments
- Provides considerable information about physical properties.

Non-Contact AFM

The unique characteristic of NC-AFM is that the surface profile is obtained by little or no contact between the tip and the sample [18, 22]. In the non contact AFM, the cantilever is made to vibrate near the surface of the sample in order to detect the van der Waals forces between the tip and the sample [18, 22]. The gap between the tip and the sample in NC-AFM is typically in the order of 50-150 angstroms (or tens to hundreds of angstroms) [18, 22]. The total force between the tip and the sample in the non contact regime is about 10^{-12} N which is low when compared to contact-AFM. So this factor of the non-contact AFM facilitates in the study of "soft" or "elastic" samples. It is also advantageous to study those samples like Silicon which should not be contaminated during the tip-sample

interaction [18, 22]. Because of the presence of weaker forces when compared to contact mode, the cantilevers used in non-contact mode are stiffer because the fluid contaminant layer present is thicker than the range of the van der Waals force gradient, and as the oscillating probe can get trapped in the fluid layer or vibrates beyond the range of the forces that it is used to detect. So this feature constitutes a limitation as the resolution of the images obtained by non contact AFM is quite low [18, 22].The small force and the high stiffness of the cantilever beams make the magnitude of the signal very small and hence difficult to measure. So this shortcoming in measuring the tip-sample distance also limits the usage of non-contact AFM to considerable extent. Hence for the reasons stated before, the NC-AFM does not suffer from tip to sample degradation effects that are sometimes observed after taking numerous scans with C-AFM. "If layers of condensed water are lying on the surface of a rigid sample, then the AFM operating in contact mode will penetrate the liquid layer to image the surface and the non-contact AFM will image the surface of the liquid layer."[18]

Intermittent Contact AFM

The intermittent contact AFM is also otherwise called as the tapping mode AFM. The mode of operation of an IC-AFM is very similar to that of NC-AFM except that in IC-AFM the vibrating cantilever is brought closer to the sample [18, 22]. It is characterized by oscillating the cantilever at its resonant frequency and the gap between the tip and the sample is reduced, in such a way that when the cantilever oscillates it just barely touches or "taps" the sample. The vibration of the cantilever is actuated by a PZT and amplitude of vibration is around 20-100 nm when the tip does not touch the sample. In the constant force mode of operation of tapping mode AFM a feedback loop keeps the oscillation of

the cantilever beam constant [18,22]. An optical system detects the change in the amplitude vibration which in turn is used in the computation of the error between this change in the amplitude and the preset value [18, 22]. Now this error signal is used in driving the PZT actuator and maintains constant amplitude of the cantilever, hence a constant force on the sample. The error signal which drives the PZT actuator in the vertical direction is used to plot the surface profile of the sample. The intermittent contact AFM is used in those cases when there is a risk of the sample with low moduli, getting damaged by the dragging of an AFM tip across its surface. IC-AFM is preferred to NC-AFM and C-AFM where there is a greater variation in the surface profile of the sample and also because it eliminates the lateral forces (friction or drag) between the tip and the sample owing to the short duration of contact of the tip with the sample [18, 22].

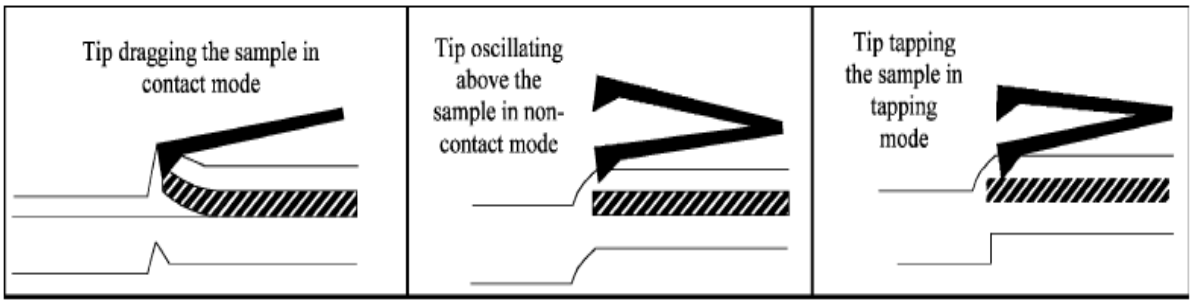

Figure 2.5: Contact mode (left), Non-contact mode (middle) and tapping mode (right) [22].

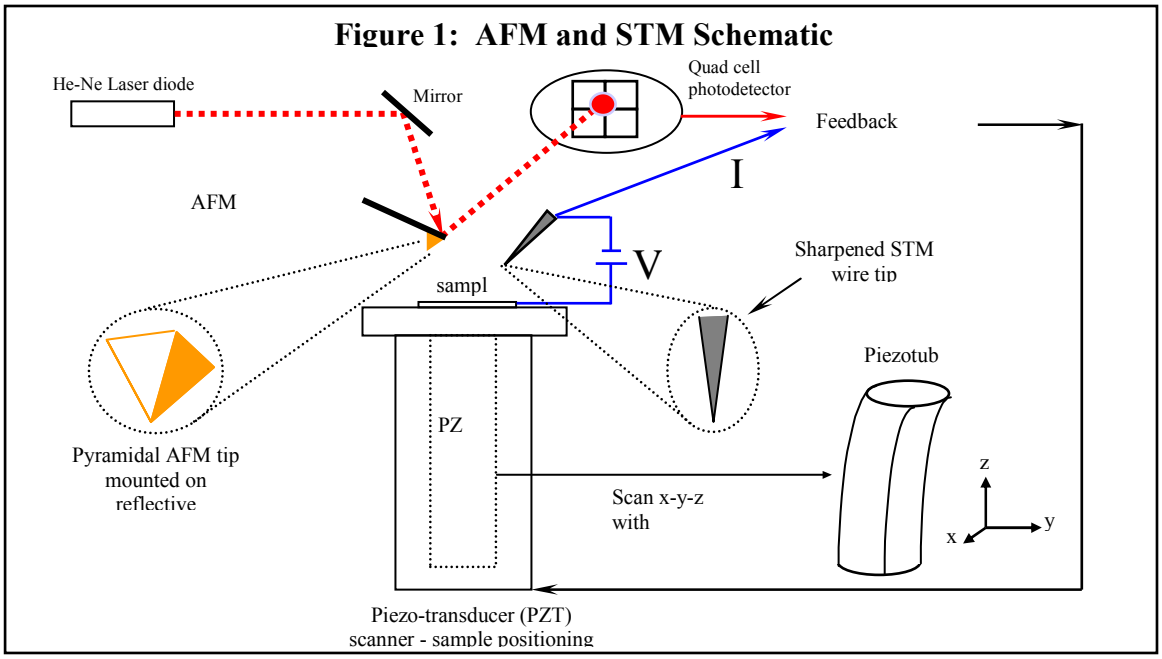

Figure 2.6: A Schematic highlighting the difference between the operation of AFM and STM [26].

Magnetic Force Microscopy

Magnetic Force Microscopy (MFM) belongs to the same genre of AFM except that this particular class of microscopy is used to image the magnetization patterns with high resolution with a nickel or iron tip which is magnetized along its length, contrary to a normal AFM (or any other force microscope) operating in the non-contact mode.

This is accomplished by minimal sample preparation [27]. The tip of a MFM is also mounted on a cantilever similar to AFM, but the difference being the tip is coated with a ferromagnetic thin film [27]. The tip to sample distance is typically 10-500nm. As the name suggests, the tip in MFM interacts with the magnetic field (which is because of the magnetic dipoles present in both the tip and the sample) emanating from the sample. MFM gives information about surface profile as well as the magnetic properties of the surface [27]. The distance between the tip and the sample determines the type of properties obtained [27]. Closer the tip is to the sample, the image gives information

about the topography of the sample and further away the distance between the tip and the sample the image gives information about the magnetic effects pertaining to the sample [20]. The detection is based on monitoring shifts in the cantilever's effective resonant frequency. The magnetic gradient present between the tip and the sample affects the effective resonant frequency and this shift in resonance frequency is caused by the change in oscillation amplitude. The MFM is essentially used in the study of the magnetic media giving insight into both head performance and quality of the storage medium [20].

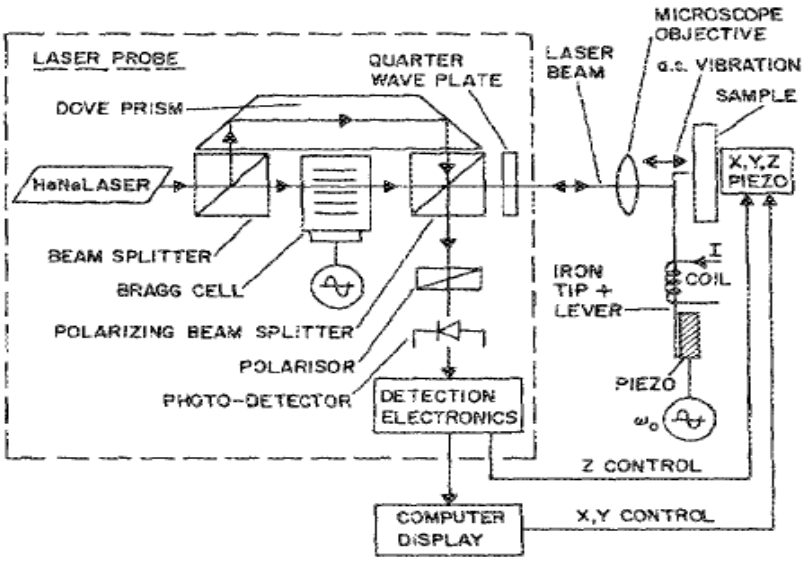

Figure 2.7: Experimental setup for mapping magnetic fields by "Force Microscopy" [28].

Scanning Capacitance Microscopy

Scanning Capacitance Microscopy (SCM) is used as an auxiliary apparatus along with AFM. The principle behind the SCM is the same as any other SPM with the only variation that a SCM images the spatial variations in capacitance [2]. The capacitance between the tip and the sample is detected using a circuit. SCM and EFM are similar in

inducing a voltage between the tip and the sample [2]. There is a capacitance that exists between the tip and the sample, this capacitance depends on the dielectric constant of the medium. Magnetic and Electrostatic forces of interaction experienced by the tip placed above a homogenous surface are given by the Equations 2.1 and 2.2 [2]:

$$F_{electrostatic} = -\frac{1}{2}(\Delta V)^2 \frac{\partial C}{\partial z} \tag{2.1}$$

$$F_{magnetostatic} = \nabla(mB_{sample}) \tag{2.2}$$

where $F(z)$ is the force, $\Delta V = V_{tip} - V_{surf}$ is the potential difference between the tip and the surface, z is the vertical tip-surface separation, and $C(z)$ is a tip-surface capacitance. From Equation (2.1) it can be inferred that capacitance is a function of the tip-surface separation, topography and tip-shape [29]. SCM is useful in the spatially resolved characterization of semi-conductor devices [2, 29]. This process of characterization is done by obtaining the C-V curves or Capacitance Voltage curves of the semi conductor surfaces [30]. The shape of the C-V curves thus obtained using the SCM are a function of the oxide thickness. The SCM data pertaining to semiconductor devices can be obtained only for devices with uniform oxide thickness [30].

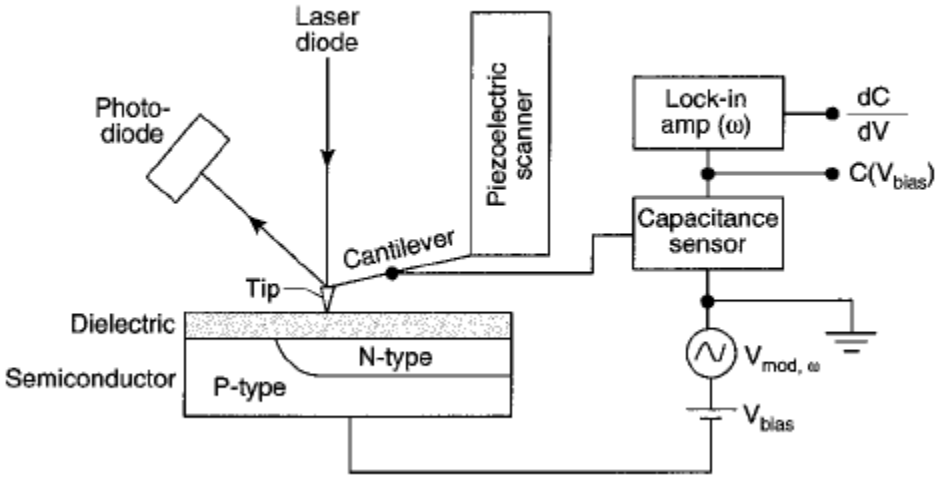

Figure 2.8: Block diagram of a SCM [31]

Lateral Force Microscopy

The cantilever during the process of scanning in contact mode is subjected to many types of forces namely lateral forces and normal forces [18]. The normal forces cause the bending of the free end of the cantilever beam in the vertical direction [2]. And the former, which is parallel to the sample surface induce lateral deflections or twisting of the cantilever [18]. These two forces are perpendicular to each other [18]. The causes of the lateral deflections are due to the change in the surface friction (owing to the in homogeneity in surface) and changes in the slope [18]. The fact that these two forces are perpendicular to each other helps in the acquisition of two types of data: one pertaining to the usual surface profile (which is common to AFM as well) and the other related to the frictional forces (which are unique to MFM) [18]. The deflection of the cantilever is measured using a Position Sensitive Photo Detector or PSPD for short [4, 28]. The PSPD consists of two types of cells: one the bi-cell and the other the quad-cell. The bi-cell is typically incorporated in AFM instrumentation, when used to measure the surface profile

of the sample [18]. The quad-cell helps in the further detection or measurement of the twisting of the cantilever. Both the “bi-cell” and the “quad-cell” basically measure the orientation as well as the bending of the cantilever by reflecting laser beams off the backside of the cantilever [18]. The reflected laser beams will travel in mutually perpendicular directions if in case both bending as well as torsion motion of the beam are measured using the “quad-cell”. The illustration in Figure 2.9 depicts the functioning of the PSPD for detecting torsion as well as bending of the cantilever beams:

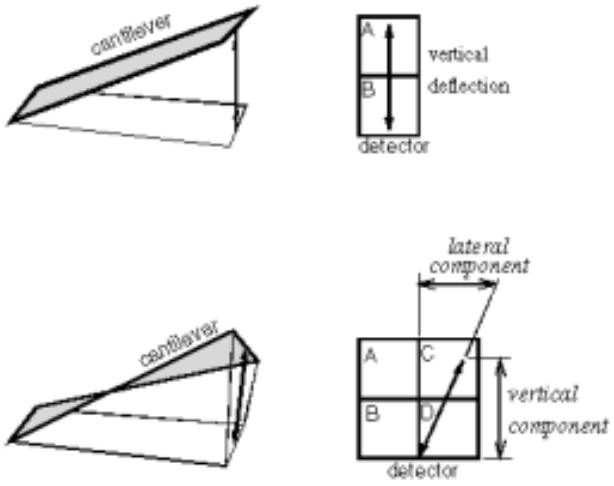

Figure 2.9: The PSPD for AFM (top) and LFM (bottom) [18]

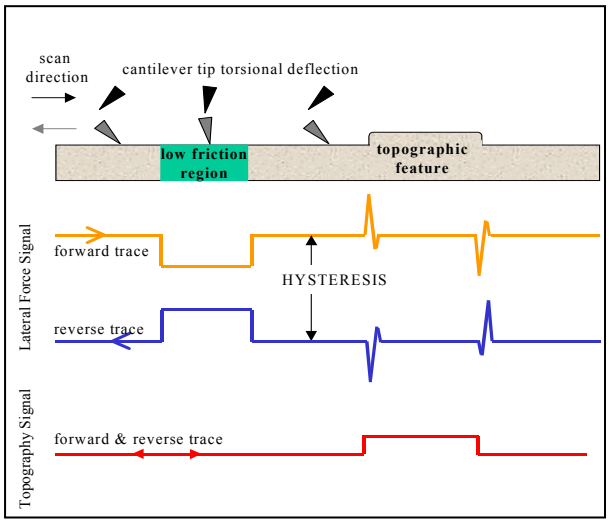

Figure 2.10 Diagram highlighting Lateral Forces [26]

Force Modulation Microscopy

Force modulation microscopy (FMM) is another variant of the class of AFM, which is similar in operation to LFM and MFM [18]. FMM is used in the study of mechanical properties of the sample [18]. The tip is in contact with the sample in the FMM. A periodic signal is applied to either the tip or the sample [18]. Elastic properties of the sample can be obtained from the change in the amplitude of the cantilever modulation [18]. A Force modulation image is obtained from the changes in the amplitude of the cantilever modulation. Figure 2.11 shows image obtained from the Force Modulation Microscope of a carbon fiber/ polymer composite:

Figure 2.11: Images of a Carbon Fiber/Polymer composite collected simultaneously field of view 5µm [18]

Phase Detection Microscopy

Phase detection microscopy, as the name suggests monitors the phase lag between the signal that drives the cantilever to oscillate and the cantilever oscillation output signal [18]. The change in the phase lag reflects the change in the mechanical properties of the sample surface like elasticity, adhesion and friction [18]. The change in the phase lag as well as topographic images are taken simultaneously, this facilitates obtaining both topographical images as well as material properties related to the sample [18]. Phase detection microscopy technique can be used in conjunction with a NC-AFM for getting both the topography images as well as phase detection information.

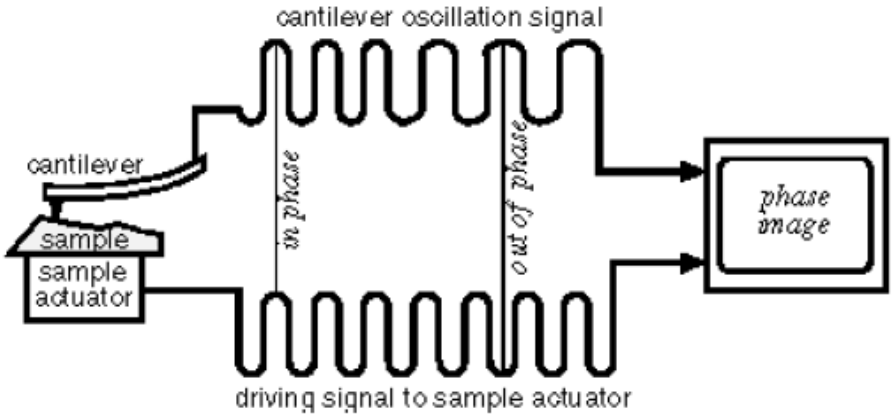

Figure 2.12: The phase lag varies in response to the mechanical properties of the sample surface [18]

Electrostatic Force Microscopy

Electrostatic Force Microscope (EFM) maps the electrically charged regions in the sample similar to Magnetic Force Microscopy (MFM), which maps the magnetic domains in the sample [18]. Both in the EFM as well as MFM a probe vibrates at its resonance frequency. In Electrostatic Force Microscopy, a voltage exists between the tip and the sample in order to image the static charges present on the sample surface [14]. The presence of these electrical charges in the sample affects the vibration amplitude of the probe. EFM is used in the study of spatial variations of surface charge carrier density and the electrical properties of the sample in general [14, 18]. EFM is used in testing the performance of microprocessor chips at sub-micron scale, the technique of which is called as "voltage probing". The microscopy technique also finds its application in determining the concentration and distribution of dopant atoms in doped silicon as the doping concentration plays a very important role in the chip performance [2]. Figure

2.13 reveals the images of a polished sapphire surface with both contact as well as electrostatic forces.

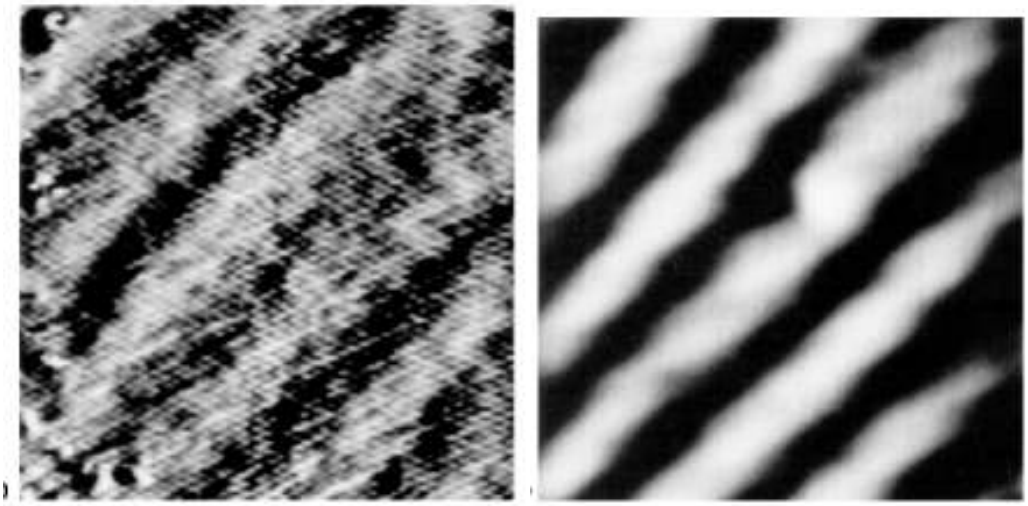

Figure 2.13: Images $(2.5\mu m \times 2.5\mu m^2)$ of a different r-cut sapphire sample with more closely spaced steps. Image 2.13 (a) Was taken using repulsive contact forces while (b) was taken using attractive electrostatic forces [32].

From image 2.13, pertaining to electrostatic forces it can be inferred that images of charge accumulations can be obtained from EFM. The most commonly used techniques of EFM are Force Gradient Imaging and Scanning Surface Potential Imaging.

Force Gradient imaging

This technique of EFM imaging is widely used commercially in the non-contact mode. A surface topography is obtained in the first scan and then the corresponding electric charge distribution is recorded in the second scan. The amplitude, phase and frequency of vibration of the tip get changed under the influence of electrostatic forces acting on the

tip. When the external tip bias is absent the force gradient acting on the tip is proportional to the product of electric field and the induced charge. “The tip can be made sensitive to electrostatic forces by biasing it with respect to the sample [14]”. When a DC voltage is applied between the tip and the sample, the force gradient that acts as a consequence on the tip is the result of various types of interactions. Those individual interactions can be determined by taking measurements at different scan heights and different tip biases. The effect of electrostatic forces acting on the tip causes a decrease in the resolution of the image obtained by EFM. This led to the development of Scanning Surface Potential Microscopy.

Scanning Surface Potential Microscopy

This technique is also alternatively called as the Kelvin Probe Microscopy (KPM). The force existing between the tip and the sample when ac tip bias is applied is given by Equation (2.3) [14]:

$$F(z) = \frac{1}{2}\frac{\partial C(z)}{\partial z}[(V_{dc} - V_{surf})^2 + \frac{1}{2}V_{ac}{}^2[1 - \cos(2\omega t)] + 2(V_{dc} - V_{surf})V_{ac}\sin(\omega t)] \quad (2.3)$$

From equation (2.3), it can be observed that when an ac bias is applied between the tip and the sample then both static components as well as harmonic components are produced. The dc component present in the biasing voltage contributes to the static components as well as to the first harmonic components. The rest of the harmonic components are induced by the presence of ac part of the biasing voltage. When the condition of $V_{dc} = V_{surf}$ is achieved then the first harmonic vanishes, under this condition the surface potential is directly measured by adjusting the tip offset potential [14]. “It is noteworthy that the signal is independent of the geometric properties of tip-surface

system and the modulation voltage. This technique allows high potential resolution." [14].

Scanning Thermal Microscopy

"Tip-sample thermal resistance as a proximity measuring technique allowed development of Scanning Thermal Microscopy as an analog of the STM for imaging insulating materials. The primary purpose of the original microscope was not to measure surface temperature but for imaging insulating materials." [33]. The Scanning Thermal Microscope (SThM) was reported to have developed in the year 1986, the year by which the Atomic Force Microscope had not still taken birth. Wickramasinghe and Williams [34, 35] developed the first SThM in order to overcome the inability of STM to scan non-conductive surfaces. The first Scanning Thermal Microscope had a thermocouple mounted on the tungsten tip of a STM. The tip of the STM was heated and brought in close proximity to the sample. The different types of tip-sample heat transfer mechanisms play a vital role in this juncture as they control spatial resolution, temperature accuracy and resolution and imaging artifacts [33]. Majumdar [33] has dealt with a detailed description about various types of heat transfer mechanisms ranging from solid-solid conduction to liquid film conduction. "When the thermal diffusion layer surrounding the heated probe overlaps the substrate, heat is transferred to the substrate, cooling the tip and signaling the presence of a surface" [34]. The difference in the thermal conductivity of solid and air surrounding the tip, heated probe is able to sense the solid i.e. the sample surface placed near the probe tip independent of its thermal characteristics [34]. Thus SThM is used in observing the thermal behavior of materials, thermal conductivity in

particular. SThM is helpful in acquiring both topographic as well as thermal conductivity data pertaining to the sample. The material used in the cantilever is sensitive to the change in the thermal conductivity of the sample. This change in the thermal conductivity in turn effects a change in the deflection of the cantilever. Similar to MFM, a topographic image is generated from the changes in the cantilever's amplitude of vibration.

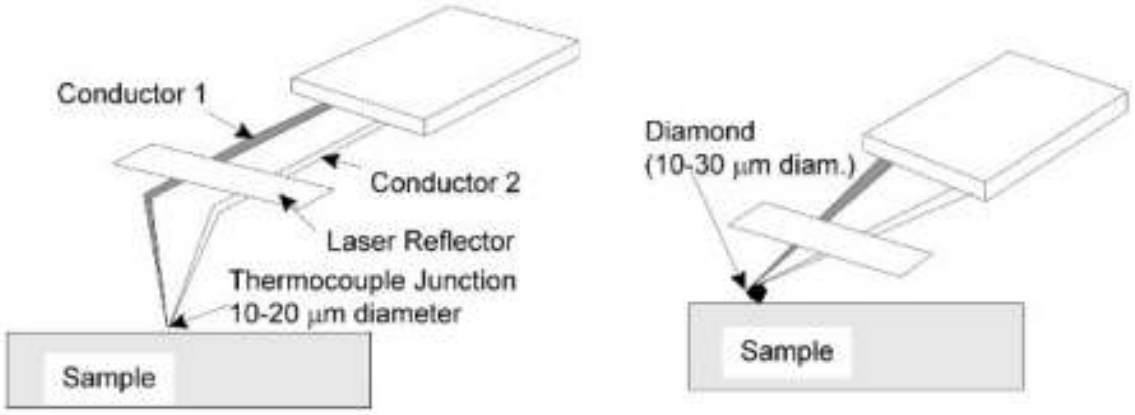

Figure: 2.14: Experimental apparatus and details of the cantilever thermocouple probe used for SThM [33, 36].

Near Field Scanning Optical Microscopy

"NSOM brings to the SPM family an optical probe than can yield complementary information to the other techniques that can only be obtained by optical mean [34]".The resolution that could be achieved by a objective lens of numerical aperture *NA* for a light of wavelength λ as proposed by Abbe' is as per Equation (2.4) [37,38]:

$$R = \frac{0.61\lambda}{NA} \tag{2.4}$$

From Equation (2.4) it can be inferred that the resolution in a conventional optical microscope is a function of the wavelength of light used. NSOM optical technique overcomes the conventional Abbe barrier or the diffraction limit [34, 39]. Compared to the wavelength of light the distance between the tip and the sample is smaller hence the name “Near field” [39].

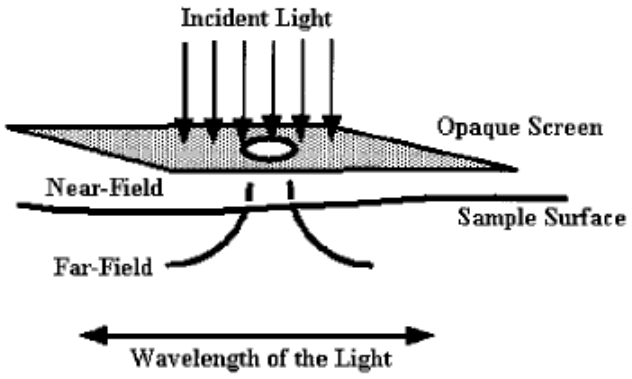

Figure 2.15 Schematic representation of Synge’s idea for achieving sub diffraction limits spatial resolution [40].

The NSOM has the advantage of possessing contrast mechanisms and high resolution which are not present in a conventional optical microscopy technique [34]. “Optical Microscopy has the advantage that it is non-invasive to the sample which makes it helpful in rendering investigative research in Biology, Medicine and Genetics in their native environment [34]”. The sample is excited by passing the light through a sub-micron aperture at the end of an optical fiber [37, 18]. The diameter of the aperture is in the order of nanometers. In order to prevent light loss the fiber is coated with aluminum or some other metal to ensure a focused beam [37, 18]. This distinguishes a NSOM from the rest of the family of SPMs in the sense that optical information (like refractive index) is

collected from the sample by the NSOM. Generally in a NSOM experiment either the tip or the sample moves up and down maintaining a constant force similar to constant current set up in a STM experiment. The up and down motion of the tip or the sample will be in accordance with the sample topography [37, 18]. Similar to other conventional SPMs the sample is moved by a PZT [37, 18].

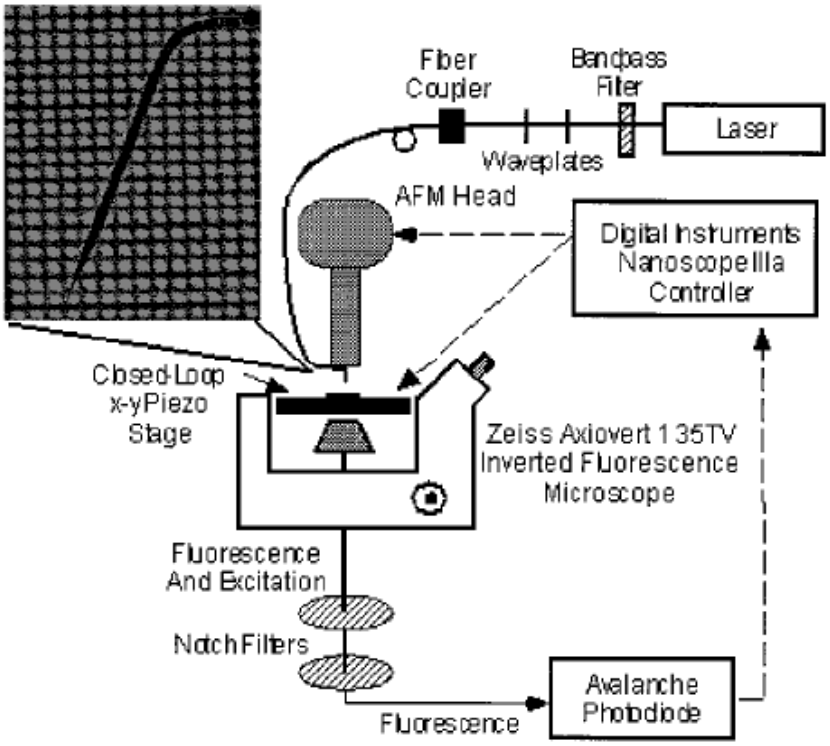

Figure 2.16: Schematic of a near field microscope built around an inverted fluorescence microscope [40].

As in any other scanning probe microscope, the tip to sample distance is monitored but they being specific to NSOM are discussed as below [39]:

- Shear Force Feedback
- Tapping Mode

Shear Force Feedback

One of the earliest methods employed were the optical techniques for determining the tip to sample proximity. The distance between the tip and the sample bears a direct relationship to the intensity of the reflected or the transmitted light from the sample. This relationship is due to the far field interference phenomenon [41, 42 and 43]. The drawback of the above technique is that it is not applicable to all samples as the optical properties of the samples acts as a criterion for implementing the technique in order to monitor the tip to sample distance. The shear force technique is "based on the observation that the amplitude of motion of a fiber probe driven at a natural vibrational resonance in a plane parallel to the sample surface decreases as the probe approaches the surface"[44]. The shear force method of detection was reported to have developed simultaneously by Betzig and co-workers and Vaez-Iravani's group [37, 44, 45 and 46]. As shown in Fig NSOM probe is dithered or laterally swayed by a piezoelectric device, parallel to the sample's surface corresponding to the mechanical resonance of the probe [37, 44]. As, mentioned before the probe is driven by a piezoelectric transducer. The resonance at which the probe is vibrated is affected by the force acting on the probe. The forces acting on the probe cause a change in the amplitude of the probe motion which in turn facilitates in determining the distance between the tip and sample [37].

Tapping Mode

The tapping mode method of feedback is relatively new compared to the earlier described techniques. " The fiber is mounted on a piezoelectric bimorph for probe modulation normal to the sample surface" [37]. Since the feedback is employed for "near field" optical scanning microscopy the amplitude of motion is small in order to ensure that the

sample is nearer to the probe and the probe makes a weak intermittent contact with the sample surface [37]. A position sensitive photo detector (PSPD) (similar to that used in Lateral Force Microscopy) is used in order to monitor the tip to sample distance." The probe is driven at a mechanical resonance, and its motion is observed via lock –in detection of the signal from the diode" [37]. This method of feedback helps in minimizing the interaction forces (which is in the order of piconewton or nano-newton range) existing between the tip and the sample [37, 47].

Chapter Summary

Scanning Probe Microscopes have revolutionized the world of microscopy techniques ever since their invention. Different types of Scanning Probe Microscopes evolved after the invention of Scanning Tunneling Microscope in 1982 and Atomic Force Microscope in 1986. The basic principle behind the various types of Scanning Probe Microscopes is the interaction of the tip and sample. Depending upon the type of interaction the Scanning Probe Microscopes are classified into various categories. Within each sub category they are further classified depending upon the modes of operation, like for example Scanning Tunneling Microscope is classified as Constant Current and Constant Height. Atomic Force Microscope is classified as Contact AFM, Non Contact AFM and intermittent Contact SFM.

CHAPTER 3

THEORETICAL MODELING OF SCANNING TUNNELING MICROSCOPY

The concept of Scanning Tunneling Microscopy evolved on the basis of electron tunneling.

Concept of Tunneling

The tunneling phenomena was experimentally observed in 1928 in the following three cases: the natural decay of certain heavy nuclei by $\alpha-$ particle emission, the ionization of atomic hydrogen in a strong electric field and, similarly the emission of electron from a cold, clean metal surface under the application of a strong electric field.[48]

From Figure.3.1, we can observe that a α particle initially with a meta-stable energy E decays exponentially after it comes out of the nucleus with a kinetic energy E_K which is of the order of a few MeV.

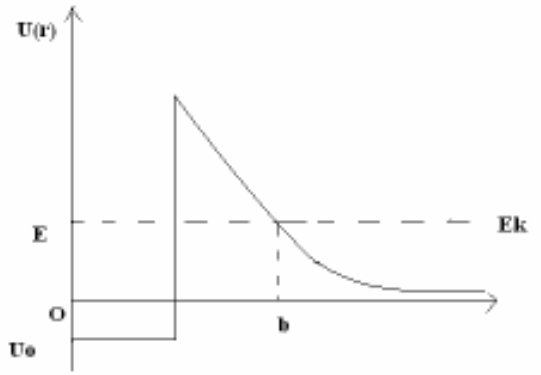

Figure 3.1: Decay of radioactive nucleus by tunneling of alpha particle through coulomb barrier. Regularity between energy E_K of emerging alpha particle and lifetime τ_α against decay substantiates tunneling model [48].

The tunneling phenomenon is attributed to the wave aspect of particles as propounded in quantum mechanics. In accordance with this effect, the electrons are given a non-zero or finite probability of passing through a forbidden energy gap. This is in opposition to the principles of classical mechanics where the electrons require energy greater than the forbidden potential energy to cross the energy barrier.

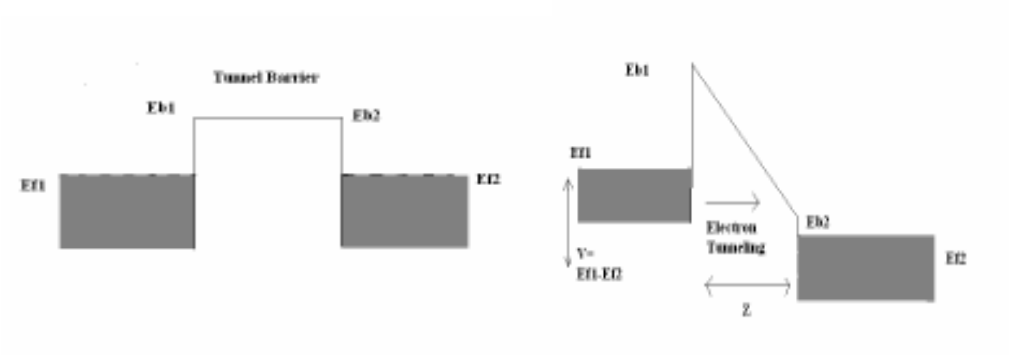

Figure 3.2: The energy levels in two solids separated by an insulating or vacuum barrier (a) with no bias applied between the solids and (b) with an applied bias. Energies of the electrons in the solids are indicated by the shaded areas up to E_{F1} and E_{F2}, which are the Fermi levels of the respective materials. The applied bias V is $E_{F1} - E_{F2}$ and Z is the distance between the two solids. [14]

The solutions to Schrödinger's equation inside the barrier have the form as [14] =

$$\psi(z) = \psi(0)e^{-kz} \tag{3.1}$$

where

$$k = \frac{\sqrt{2m(V-E)}}{\hbar} \tag{3.2}$$

Where m is the mass of an electron, $\hbar$ is the reduced Planck's constant, E is the energy of the electron; V is the Potential in the barrier.

Tunneling Probability

As mentioned before, the tunneling processes propounded under the precincts of quantum mechanics follows directly from the solutions of Schrödinger's equation (Equation. 3.1) and the probability is interpreted by $\psi^*\psi$ [48].

The rate at which such processes occur can be calculated from the Wentzel-Kramers-Brillouin (WKB) approximation as per equation (3.3) [48]

$$D = e^{(-2K)} \tag{3.3}$$

$$\text{where } K = \int_{x_1(E_x)}^{x_2(E_x)} \kappa(x, E_x).dx \tag{3.4}$$

$$\text{where } \kappa(x, E_x) = \left\{ \frac{2m^*[V(x) - E_x]}{\hbar^2} \right\}^{1/2} \tag{3.5}$$

The decaying probability of the electron through the barrier is proportional to the tunneling current which in turn is exponentially dependent on the barrier width as per Equation (3.6):

$$P \propto I \propto e^{-2kz} \tag{3.6}$$

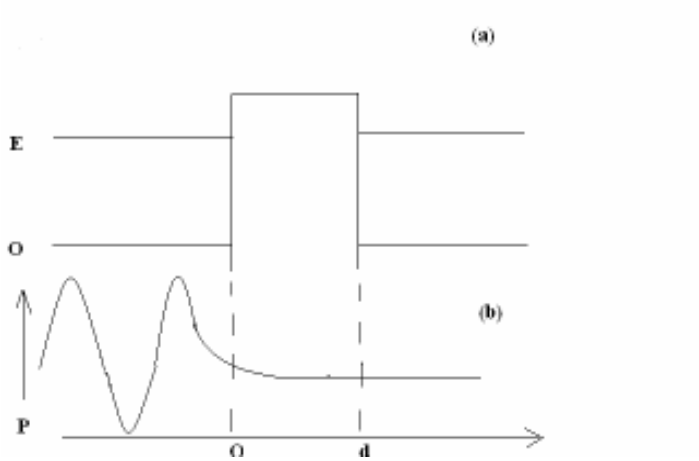

Figure 3.3 (a) A simple rectangular barrier potential of height ϕ_O (b) The probability density function P for typical (rectangular) barrier penetration [49]

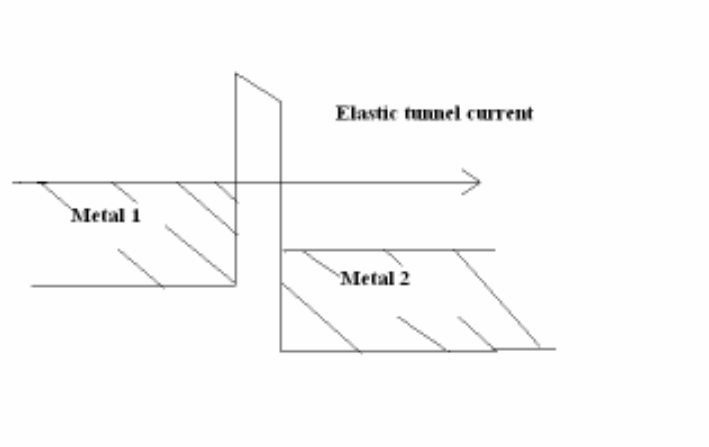

Figure 3.4: Metal-insulator- metal tunnel junction. Two metal electrodes at T=0 K. The electron energy levels are filled up to the Fermi energy. Electrons in the occupied states of the left electrode may tunnel elastically to the empty states of the right electrode [49].

The net current flow across the metal-insulator-metal junction constitutes the tunneling probability contributed by the conduction electrons which possess energies up to the Fermi energy. The parameter transmission coefficient indicates the probability of an

electron passing through a potential barrier [50]. The probability depends on the shape of the barrier (rectangular, triangular, etc.), on its width and height.

Hence for a lower and thinner barrier, higher is the transmission coefficient. For a rectangular barrier the transmission coefficient is given by:

$$T = \frac{1}{1 + \frac{1}{4}\frac{V^2}{E(V-E)}\sinh^2\left(\frac{a}{h}\sqrt{2m(V-E)}\right)} \tag{3.7}$$

Where "*a*" and "*h*" are the width and the height of the potential barrier, respectively, and E is the energy of the electron (E<V) [51].

Fermi's golden rule states that [52].

"The transition rate i.e. the probability of transition from an initial state $\psi(i)$ into all final states $\psi(f)$ per unit time, is obtained by multiplying the absolute square of transition amplitude by the density of final states at the energy E_i of the tunneling electron $\sum_f \delta(E_f - E_i)$ and the pre-factor $\frac{2\pi}{\hbar}$. The transition amplitude is evaluated as the matrix element of some transition inducing potential between the initial state $\psi(i)$ with energy E_i and the final state $\psi(f)$ with energy E_f respectively. The initial state is the wave function containing the electron before the transition and the final state is the wave function of the electron after the transition ". Kinetic energy of the electron in a direction perpendicular to the barrier affects the tunneling probability.

Current Density

The current density is calculated as [60]:

$$J = \frac{2e}{\hbar}\sum_{K_t}\int_{E_Z} P(E_Z)[f(E) - f(E+eV)]dE_z \tag{3.8}$$

The Equation (3.8) is applicable for a free electron model.

From Equation (3.8) we can observe that the probability of tunneling is a function of the kinetic energy E_z, when the motion is perpendicular to the barrier and the Fermi occupation function depends on the total energy of the electron and the applied bias voltage [60]. So the total current density is the contribution of the electrons with the same E_Z and hence the same $P(E_Z)$ over K_t [60]

These states can be illustrated (fig 3.5) as lying on annulus or disc in k-space as shown in the fig and hence the total current density at T=0K becomes as per equation (3.9) [49]

$$J(v) = \frac{4\pi me^2 V}{\hbar^3}\int_0^{E_F - eV} P(E_{Z,}V)dE_Z + \frac{4\pi me}{\hbar^3}\int_{E_F - eV}^{E_F}(E_F - E_Z)P(E_Z,V)dE_Z \tag{3.9}$$

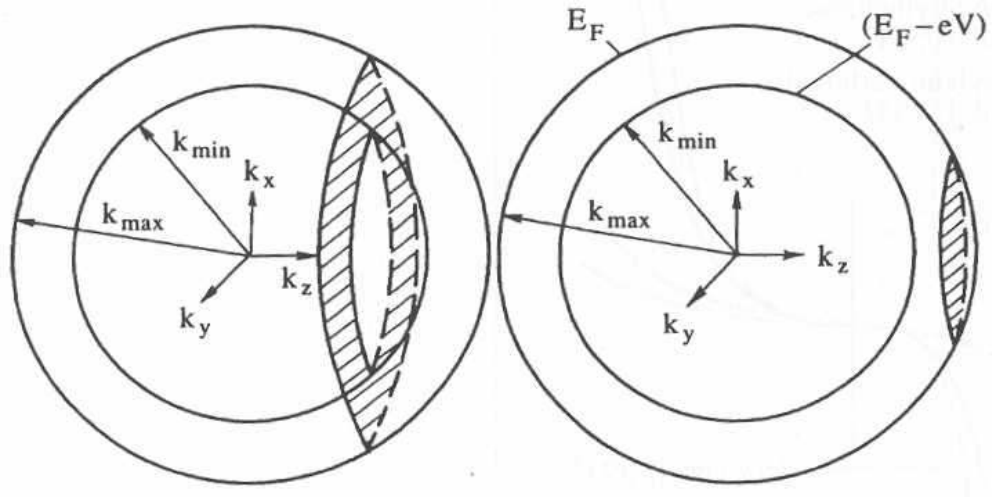

Figure 3.5 States of constant tunneling probability for (a) $k_z <= k_{\min}$ (b) $k_{\min} <= k_z <= k_{\max}$

Where the probability is constant and establishes a linear relationship between the current and the applied bias at low voltages. But for the larger voltage when the magnitude becomes a significant fraction of the barrier height, the relationship given by the equation (3.9) holds good.

Bardeen's General Formalism

Origin of the Transfer Hamiltonian Theory

Bardeen used the transfer Hamiltonian theory to explain the phenomenon of observation of tunneling current flowing between the two metals that were superconducting and were separated by thin oxide layer in Giaver's experiment in 1960 [53, 54,55].

The basis of the Bardeen's Hamiltonian theory is the quantum mechanical treatment of the electrons as wave functions which do not drop to zero abruptly at the surface of the barrier but extend into the barrier with an exponentially decaying tail [53, 52]. The process of tunneling occurs when these wave functions from the metals overlap and the electrons can cross the barrier [53, 52]. The effect also takes into account many body effects and band structure surface states. [52, 56, 57]

Hence in the case of Hamiltonian, the total structure of the base and the sample can be separated into different subsystems with known Hamiltonians and wave functions as in Figure 3.6 [52, 56].

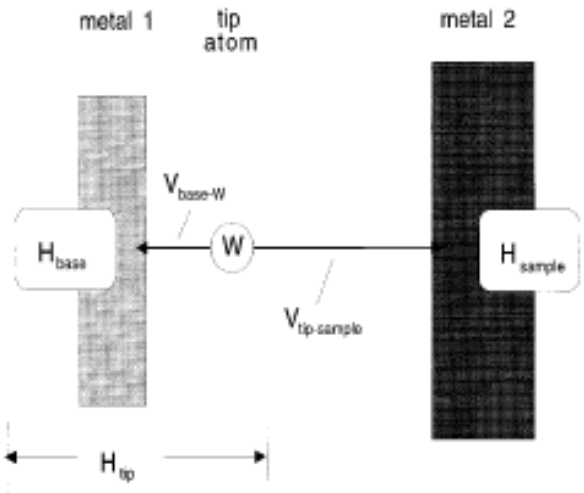

Figure 3.6: Schematic representation of the STM Hamiltonian [56]

$$H = H_0 + H_{sample} + V_{tip-sample} \tag{3.10}$$

$$H = H_{base} + V_{atom-base} + H_{atom} + H_{sample} + V_{tip-sample} \tag{3.11}$$

In equation (3.10), H_0 describes the non interacting tip plus sample surface. The tip is considered as a tungsten atom or an Al atom adsorbed on a flat W surface. Bardeen's formalism leads to the evaluation of the matrix element $M_{\mu v}$ which is given by Equation (3.12): [58]

$$M_{\mu v} = \frac{-h^2}{2m} \int \vec{ds} (\psi_\mu \nabla \psi_v - \psi_v \nabla \psi^*_\mu) \tag{3.12}$$

where the integral is over any surface lying entirely within the vacuum (barrier) region separating the two sides. The quantity in parentheses is simply the current operator [59, 58, and 2]. So from Equation (3.12) we can observe that the integrand continues to have the wave functions ψ_μ and ψ_v of the individual systems and not the full system Hamiltonian or wave function. The main assumption behind this formalism is that the

tunneling process is contributed by the wave functions of the two sub systems which are unperturbed. The above method is uncomplicated and easy for computation [55].To obtain the total transition conductivity $\gamma(E)$ at the tunneling energy E, one has to sum over all possible initial and final states at this energy. Within the approximation of non interacting tip electrode and sample surface, the transition conductivity for an electron tunneling at energy $E_f = E_i$ is introduced in the perturbation limit as: [52]

$$\gamma(E) = \frac{4\pi e^2}{\hbar} \sum_{i,f} \left| \langle \psi_f | V_{curr} | \psi_i \rangle \right|^2 \delta(E - E_i) \delta(E - E_f) \tag{3.13}$$

Where

$$V_{curr} = V_{base-W} + V_{tip-sample} \tag{3.14}$$

The transition conductivity evaluated in Equation (3.13) was for the energy corresponding to the tunneling energy E. Moreover, the applied voltage does not determine the transition conductivity. But for tunneling energies near the fermi level and the applied voltage tending to zero, the transition conductivity is just the inverse of the resistance R. [52]

$$\gamma = \frac{dJ}{dU} \text{ at } E = E_{fermi} \tag{3.15}$$

Drawbacks of Transfer Hamiltonian

The inherent drawbacks in the transfer Hamiltonian theory is that the coupling between the tip and the sample surface in the STM configuration has been neglected and hence the validity of Transfer Hamiltonian (TH) formalism is limited in providing a consistent explanation for the observed STM images[60]. And to substantiate this conclusion is the

limitation of TH theory in interpreting the unforeseen large corrugations which were observed in close packed metal surfaces such as Au (111) [62] and Al (111) [61]. TH formalism gives a scope for wave functions such as the "S-wave orbital" for a spherical tip to give non zero current which is in contradiction to the concept of quantum mechanics [49].

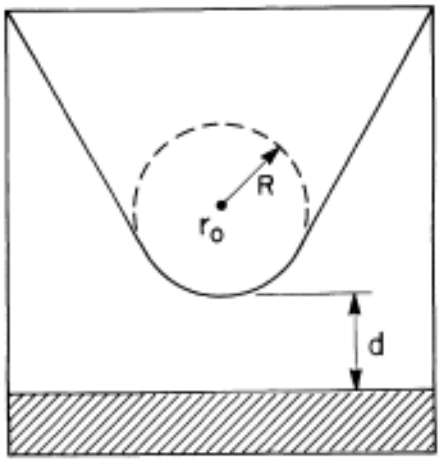

Figure 3.7: Schematic Picture of tunneling Geometry, Probe tip has arbitrary shape but is assumed locally spherical with radius of curvature R, where it approaches nearest to the surface (shaded). Distance of nearest approach is d. Center of curvature of tip is labeled $\overrightarrow{r_O}$ [58, 2].

According to Bardeen's formalism discussed earlier the tunneling current to the first order is given by [59, 2]

$$I = \frac{2\pi e}{\hbar}\sum f(E_\mu)[1-f(E_V+eV)]\left|M_{\mu.V}\right|^2 \delta(E_\mu - E_V) \tag{3.16}$$

where $M_{\mu\nu}$ is the tunneling matrix

f (E) = Fermi function

V= applied voltage

E_μ = Energy of the state ψ_μ in the absence of tunneling [59].

For room temperature and at small voltages of around ($\cong$ 10 m eV), we take the limits of small voltage and temperature as [59]:

$$I = \frac{2\pi e^2}{\hbar} V \sum_{\mu,\upsilon} \left| M_{\mu\nu} \right|^2 \delta(E_\nu - E_f)\delta(E_\mu - E_F) \tag{3.17}$$

On the basis of above formalism, Tersoff and Hamann [59, 58] proceeded with their derivation of *I*.

Tersoff and Hamann [59, 58, 63, 2] is an independent electrode approximation in which the tip is modeled as a locally spherical potential well where it approaches nearest to the surface as shown in the figure 3.7. Tersoff and Hamann [59, 58, 63, and 2] help in the evaluation of the tip wave function which is given as:

$$\psi_\mu = \Omega_t^{-1/2} C_t kRre^{kR} (k\left|\vec{r} - \overrightarrow{r_0}\right|)^{-1} e^{-k\left|\vec{r}-\overrightarrow{r_0}\right|} \tag{3.18}$$

Where Ω_t = Probe Volume

k= $\frac{\sqrt{2m\phi}}{\hbar}$

The surface wave function is also expressed as:

$$\psi_v = \Omega_s^{-1/2} \sum_G a_G \exp[-(k^2 + \left|\overrightarrow{k_{11}} + \vec{G}\right|^2 z] \exp[i(\overrightarrow{k_{11}} + \vec{G})\overrightarrow{X}] \tag{3.19}$$

Equation (3.12) [50] gives $M_{\mu\upsilon}$

Now substituting the surface and the tip wave functions in the expression for tunneling matrix and evaluating the expansion term by term in *G*, we get:

$$M_{\mu\upsilon} = \frac{\hbar^2}{2m} 4\pi k^{-1} \Omega_t^{-1/2} k \,\mathrm{Re}^{kR}\, \psi_v(\overrightarrow{r_o}) \tag{3.20}$$

Now substituting (3.20) into equation (3.17), we get equation (3.21) [58, 59, 63 and 2]:

$$I = 32\pi^3 h^{-1} e^2 V \phi^2 D_t(E_F) R^2 k^{-4} e^{2kR} * \sum_v \left|\psi_v(\overrightarrow{r_o})\right|^2 \delta(E_v - E_F) \tag{3.21}$$

Where D_t=density of states per unit volume of the probe tip.

Now the final result after the substitution of the metallic values into (3.22) we get the tunneling conductance as [59, 63 and 2]

$$\sigma = 0.1 R^2 e^{2kR} \rho(\overrightarrow{r_o}, E) \tag{3.22}$$

$$\rho(\overrightarrow{r_o}, E_F) \equiv \sum_V \left|\psi_V(\overrightarrow{r_o})\right|^2 \delta(E_v - E) \tag{3.23}$$

The above analysis is applicable for large tip-sample distances. The factor $\rho(\vec{r}, E_F)'s$ behavior affects the performance of STM in terms of sensitivity of the analysis put forth by Tersoff and Hamann [52, 58, and 59]. It helps in establishing a direct relationship between STM image that has been obtained experimentally with not only the topography of the sample surface but as well with electronic structure. Any change in corrugation is directly affected by any change in the distance between the tip and sample surface which can be inferred from the relationship derived above. For periodic structures the measured corrugation amplitude decreases exponentially with resolution. The significant drawback of the above theory is the inability to explain the spatial resolution when the distance between the tip and surface is significantly large. [52, 58, 59].If $\rho(E_F)$ contains a node the current will drop to zero and the tip will be pushed into the sample by the feedback system. The node leads to an anonymously high measured corrugation.

Tersoff and Hamann [52, 58, and 59] mimic the sample charge density by a sum of spherical densities of the form $\frac{c}{r}\exp(-2kr)$ and thus obtain sample charge density as:

$$\Delta z \cong \frac{2}{k}\exp[-2(\sqrt{k^2+\frac{\pi^2}{a^2}}-k)z] \tag{3.24}$$

Where "a" is the distance between the 2 atoms, V is the height of the potential in the barrier, E_F is the Tunneling Energy. The basis on which the Tersoff-Hamann theory has been developed is that the tip is a spherical s type tip and that it helps in the evaluation of the tunneling matrix based on the surface wave functions of the tip and the sample. In the evaluation of the tunneling matrix the volume integral has been replaced by surface integral [52, 64].

Three dimensional scattering theory of scanning tunneling microscopy

The phenomenon of tunneling can be defined with respect to the scattering process in which an electron incident from the interior of the tip metal scatters at a barrier junction and has a certain probability of penetrating into the sample surface. The total Hamiltonian has the form as: [52, 53, and 54]

$$H = H^o + V_{tip} \tag{3.25}$$

$$H^o = \frac{-\hbar^2\Delta}{2m_e} + V_{cap} \tag{3.26}$$

Where H^o is the Hamiltonian of a 2 electrode system (capacitor) without tip atom, m_e is the electron mass, V^{cap} is the potential of the capacitor which includes the two electrodes,

and V^{tip} is the potential induced by a tip atom, which would break any spatial symmetry that might exists for the two electrode system [53]. The exact formulation in scattering theory is to calculate the total current of the scattering wave function $|i+\rangle$ from the generalized Ehrenfest theorem (GET). [52, 54]

$$J(i) = \frac{2\pi e}{\hbar} \sum_{f} \left| \langle f_{cap} | V_{tip} + V_{sample} \quad | i+ \quad \rangle \right|^2 \delta(E_F - E_i) \tag{3.27}$$

Where $|f\rangle$ is a current carrying state in the sample metal (the states are labeled by the incident momentum i and the final momentum f, respectively) [53, 65]. Equation (3.27) holds good for a single electron scattering. In order to obtain the net tunneling effect, the summation is applied to all the electrons. The scattering process is described by a wave function i+ which is an Eigen function of the total Hamiltonian H including the sample and tip potential and the potentials in the nano complex [52]. Here nano complex indicates the adsorbed particles along with atoms and particles in the tunnel gap that form the tip apex. i denotes the momentum of the incoming electron and + sign indicates the incoming scattering boundary conditions. Therefore <i+> describes a wave with plane components propagating from the interior tip of the electrode towards the tunnel junction and with the scattered wave components emerging from the scattering process [52].

The wave function f_{cap} contains the final momentum of the outgoing scattered electron, when it has passed through the sample, and this does not experience the potential V^{tip} in the barrier region. $\langle f|$ has to be an Eigen state of H_o satisfying the outgoing scattering boundary conditions i.e. $\langle f|$ describes a wave with plane wave components running away from the tunnel junction in the direction towards the interior of the sample and

scattered wave components collapsing towards the scattering process[52].

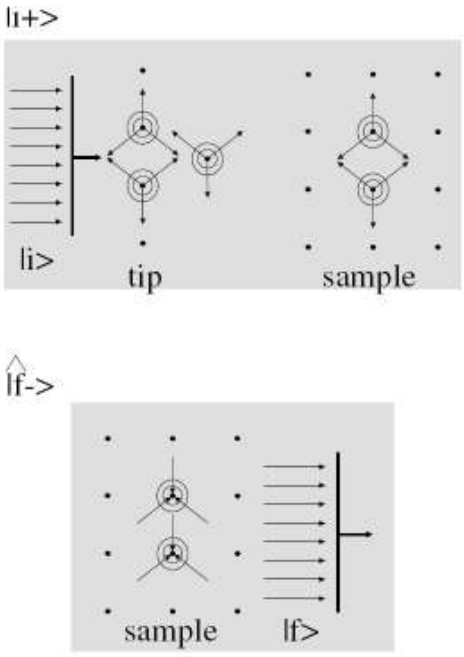

Figure 3.8: Boundary Conditions for STM scattering process [52]

The GET [65] provides a natural connection between the mathematical and physical descriptions of the collision process and it enables the resolution of the scattered amplitude in any channel to be effected quite readily [51, 58]. So using that the current is obtained as:

$$J_{f\leftarrow i} = \frac{4\pi e}{\hbar}\left|\left\langle f\left|V_{curr} + V_{sample}\right.\right|i+>\right|^2 \delta(E_f - E_i) \tag{3.28}$$

In Equation (2.8)

$$V_{curr} = V_{apex-base} + V_{apex-sample} \tag{3.29}$$

By substituting the unperturbed tip wave function $|i\rangle$ instead of $|i+\rangle$, then Bardeen's formalism can be obtained from the GET in first order perturbation theory [51].

When the applied bias is opposite then the tunneling current becomes as:

$$J_{f\leftarrow i} = \frac{4\pi e}{\hbar}\left|\left\langle f\left|V_{curr} + V_{base}\right|i+\right\rangle\right|^2 \delta(E_f - E_i) \tag{3.30}$$

Elimination of V_{sample} in the evaluation of the scattering states

It has been proved [58, 52] mathematically that transition matrix contains the Eigen states of the H_{sample} instead of the plane waves. It is because of the fact that the scattering effects are already incorporated in the sample and hence V_{sample} is eliminated from the transition matrix element. Further analysis have also been presented in the paper [52] in this regard, where it has been concluded that for a sufficiently large number of atomic layers in the tip base and in the sample the tunneling current is not dependent upon what is happening far from the tunnel junction. Adding all the transition matrix elements we get the total current using the Gellman and Goldberger theorem[58, 52] as:

$$J = \frac{4\pi e}{\hbar}\sum_{f,i}\left|\left\langle \hat{f}-\left|V_{curr}\right|i+\right\rangle\right|^2 \delta(E_F - E_i) \tag{3.31}$$

Where $\left\langle \hat{f}-\right|$ is an Eigen state of H_{sample} (H_{base}) for tunneling into the sample (the tip).

The transition matrix used in GET is as per equation (3.32):

$$< \hat{f}-\left|V_{curr}\right|i+>= \sum_A V_{fA}\left\langle A\right|i+\left.\right\rangle \tag{3.32}$$

Where $\left\langle A\right|i+\left.\right\rangle = \sum_B (1 - G_{cap}V_{curr})_{AB}^{-1}\left\langle B\right|i_p\left.\right\rangle$ (3.33)

G_{cap} is the Green operator for the system comprising the 2 electrodes (base and sample in figure 3.6)

[20]When the applied voltage $\Delta E / e$ tends to zero we get J as:

$$J = \lim_{\Delta E \to 0} \frac{2\pi e}{\hbar} \frac{1}{\Delta E} \sum_{A,B,C,D} \delta_{AB}{}^{tip} \delta_{CD}{}^{cap} \widetilde{V}_{BC} \widetilde{V}_{DA} \tag{3.34a}$$

With $\delta_{AB}{}^{tip} = \sum_{i} \langle A | i+ \rangle \langle i+ | B \rangle$ (3.34b)

$$\delta_{CD}{}^{cap} = \sum_{f}^{capacitor} \langle C | f_{cap} \rangle \langle f_{cap} | D \rangle \tag{3.34c}$$

$\delta_{AA}{}^{tip}$ represents the projection of the local function $|A\rangle$ on the scattering Eigen states that are emitted from the tip and reach the sample surface. Hence it is given the name tip projected local density (TIP-LOD) [58, 52]. Similarly δ_{AA}^{cap} is called the capacitor projected local density (CAP-LOD) which is the projection of the local state on eigen functions of the two electrodes system without tip atom and gives an insight into the electronic structure of the sample on the other hand TIP LOD spells out details about the tip sample interaction [58, 52].

The $|f_{cap}\rangle$ and $\langle i+|$ factors are substituted by $|K_{sample}\rangle$ and $|K_{tip}\rangle$ which represent eigen functions of standing waves because of their non-interaction between the tip and the sample [58, 52]. Because of this substitution the GET reduced to Fermi's golden rule. Since the 3-D Scattering theory of tunneling is quite an exhaustive subject in itself to deal with, so for further analysis and treatment of the subject the readers are referred to other papers [52, 58, and 65] for 3-D scattering theory based on GET.

Chapter Summary

The theoretical modeling of interaction between the tip and sample of a Scanning Tunneling Microscope has been an area of intense research in the domain of Nanophysics. In Chapter 3 an attempt has been made to discuss about the phenomenon of tip to sample interaction based on the Bardeen's General Formalism and the three dimensional scattering theory. Chapter 4 talks about the experimental set up and the different sub systems that constitute the STM test bed.

CHAPTER 4

DESIGN AND INTERFACE OF THE EXPERIMENTAL SET UP

The STM Experimental Set up acts like a test bed for testing of the various types of controllers starting from simple linear controller to complicated non linear controller. Before the description of the experimental set up a brief overview about the design criteria to be followed in the design of the STM would help in throwing some light on the design of the STM test bed.

As mentioned earlier, the tunneling current is exponentially dependent upon the distance between the tip and the sample [66]. Hence the vibration isolator suppresses the change in the distance between the probing metal tip and the sample due to the external mechanical vibration [67]. During the operation of STM in the constant current mode the observed atomic corrugation especially that of metals will be around $0.1\,\mathring{A}$ so the objective of the vibration isolation must be at-least $\approx 0.01\,\mathring{A}$ or less [66]. The behavior of an STM as a result of the external noise is the result of two factors: the amount of vibrations which reach the STM and the response of the STM to those vibrations. [54]. Hence the need for a good vibration isolation set up is imperative based on the above arguments.

Types of disturbances to which the STM is subjected

The two types of disturbances to which the STM will be subjected are in general [66]: vibration and shock. Vibrations are repetitive and continuous in nature. Shock is defined

as a transient condition whereby kinetic energy is transferred to a system in a short time period. Buildings vibrate at frequencies between 10 and 100 Hz [68]. The excitations of the vibrations are caused by those machines which run either at or near the line frequency. The resonant frequency of vibration of the frame, walls and floors of a building, which undergo shear and bending (membrane) vibrations are typically between 15 and 25 Hz [68]. Vibrations due to ventilation ducts, transformers and motors are at frequencies between 6 and 65 Hz. The vibrations induced due to people walking are between 1 and 3 Hz [54 and 68]. From [68], it is understood that in order to offset the influence of vibrations on the performance of STM, the focus should be on the frequency range between 1 and 100 Hz.

Vibration Isolation Techniques Used

The vibration isolation technique used by the inventors was that of a magnetic levitation of permanent magnets on a superconducting lead bowl [54]. [69] The two types of vibration isolation techniques in practice are spring suspension with magnetic damping and the second is a stack of stainless-steel plates with Viton dampers between each pair of steel plates. The vibration isolation system for simplification has been subdivided into two parts one the tunneling assembly and the other the isolator table [69]. The objective of the vibration isolation is to make the two Eigen frequencies completely different from one another [69]. [70]The three types of vibration isolation in vogue are: magnetic levitation utilizing the Meissner's effect of super conductivity, a two stage coil spring suspension and multiple stacked metal plates with rubber pieces among them. The factor which prevents the usage of magnetic levitation is that it requires liquid He and requires much more elaborate vibration isolation techniques and the conventional usage of the

thermal isolation is insufficient the thermal stress takes a longer time to relax causing thermal drift in the STM Images. It is seen that the metal stack isolators are more widely used. For the STM experimental set up that has been fabricated in the Smart Structures Nano-Electromechanical Systems lab, Clemson University an optical bench bought from Newport ® has been used to damp out the vibrations. One of the earliest researches in the field of design of STM involving various criteria was dealt by Dieter W. Pohl [68].

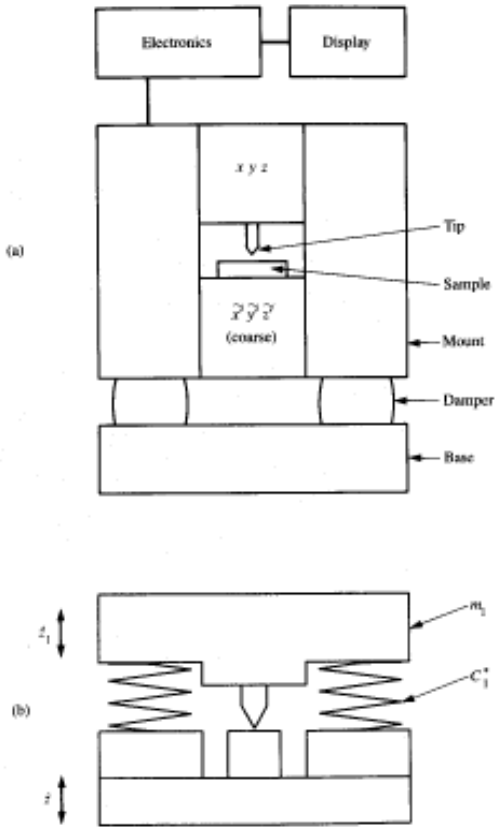

Figure 4.1: (a) Basic Features of a typical STM including two sets of three dimensional translational stages and dampers. (b) Simple equivalent model [68].

Experimental Setup

The experimental set up mainly consists of a coarse positioner (in the form of a micropositioner), fine positioner (in the form of a nano stager), STM Electronics (STM

Preamplifier), Optical Subsystem (in order to facilitate the coarse as well as the fine positioner) and STM head (constituting STM tip holder and sample holder). The detailed description about each one of them is found as below:

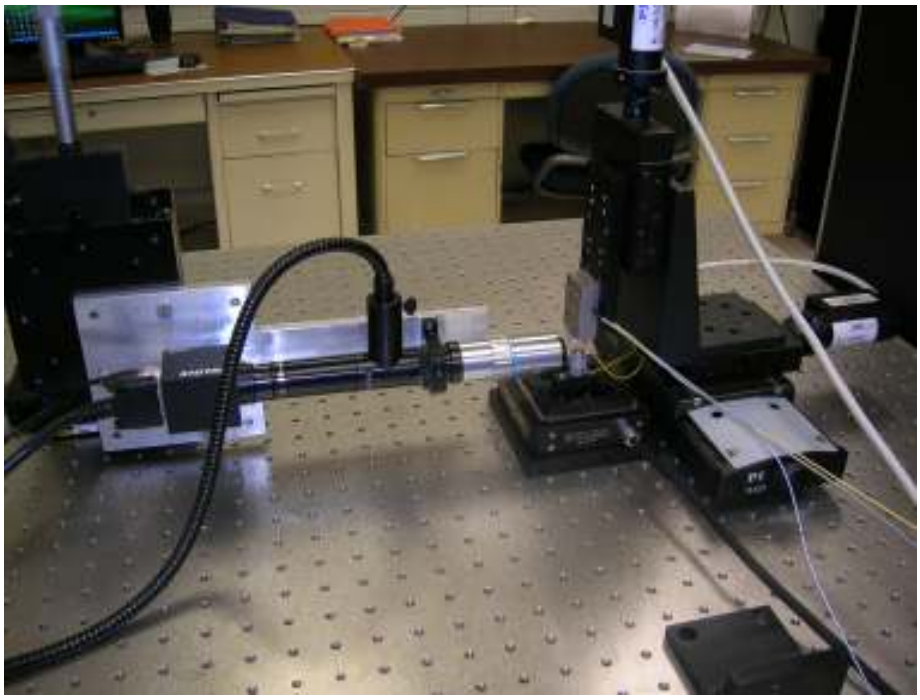

Figure 4.2: Schematic of the overall experimental set up.

Coarse Positioner

The coarse positioner is in the form of a stager with a motion in terms of micrometers. The stagers are driven by armature controlled DC servo micro motors. The micromotors are manufactured by Faulhaber®. Three micro motors interfaced with one another provide coarse movement in the X, Y and Z directions. The 3-Degree of freedom (DOF) is achieved through two micro motors of the M-126 DG1® genre in the Y and Z directions and through a single M-410 DG1® micromotor in the X direction. Further information regarding the features of the micropositioner can be found in appendix.

Fine positioner

The fine positioner is in the form of a Nanostager bought from Physik Instrumente®. The Nano positioner similar to the micro-positioner, is capable of movement in all the three directions viz X, Y and Z. The P-753® Nano Automation stage actuator from PI acts as the fine positioner in the Z direction. The P-733® single module, XY Piezo flexure Nanopositioner® and Scanner stager provides the X and Y axes movement.

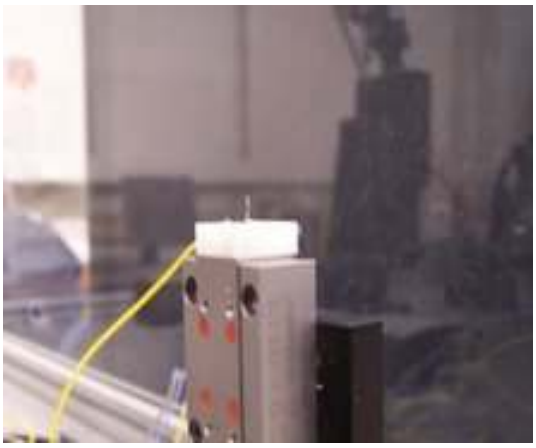

Figure 4.3: An STM tip and tip holder mounted on the P-753 Nano-automation stage actuator.

The scanning range provided by them is around 100 X 100 μm and similar, to P-753 Nano Automation® stage actuator the sub-nanometer and nanometer level accuracy is obtained owing to the capacitive feedback sensors. A detailed and in-depth analysis of the mathematical modeling based on hysteresis of the above mentioned piezoelectric actuators has been done in [70].

STM Head

The STM Head comprises of STM Tip, Tip holder and the sample holder. STM tip made with a concentration of 80% Platinum and 20 % Iridium has been used for initial imaging purposes. The in-house STM under consideration is one to be used in air. Hence the STM tip bought from Molecular Imaging Corporation® is intended to meet the objective quite well.

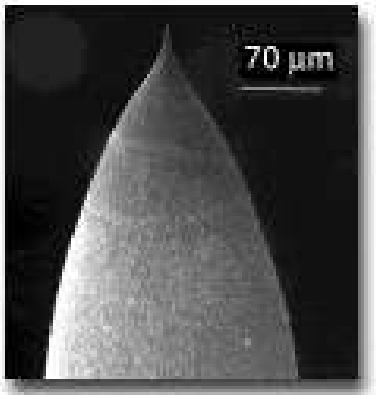

Figure 4.4: A detailed field of view of an electrochemically etched tip [71].

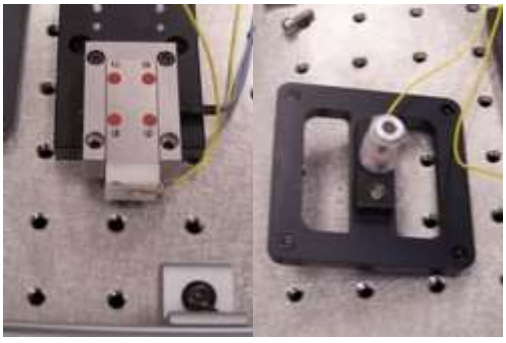

Figure 4.5: STM Head constituting the Tip Holder and the sample Holder.

The next component of the STM Head being Sample Holder was bought from Nanosurf® which was custom made specifically for use in easy Nanosurf® Air STM. This necessitated the design of a fixture for fixing the Sample Holder. This particular Sample Holder was chosen for its cylindrical shape and stainless steel body which provides better electrical contact, facilitating better application of bias voltage with lesser conduction losses. The sample holder also possesses a magnetic head on top of which a sample plate can be affixed. On a preliminary basis the sample to be imaged can be a HOPG or Graphite. The tip holder that was fabricated was taken care to be a non –conducting one so that the tunneling current losses are minimal.

STM Electronics

The STM Preamplifier forms a part of the STM Electronics. The operational ability of the STM preamplifier determines the imaging capability and the resolution of the STM Images [72]. There are two kinds of tunneling current preamplifiers which are:

a) "feedback pico-ammeter consisting of an operational amplifier with resistive feedback
b) Electro meter amplifier which consists of shunt resistor followed by a voltage amplifier realized by an op-amp as well."[72]

As mentioned in Chapter 2, the tunneling current acts as a feedback signal in the control of the Z height of the scanner in the constant current mode. The preamplifier's output acts as a feedback signal which will be utilized in the development of the controller for the

STM and the output voltage of the preamplifier changes with distance between the tip and the sample

The preamplifier circuits given in [72], [73] and [74] were tested experimentally as well as simulations was run for the same. Out of them the design specified in [74] was chosen for the STM test bed owing to its simplicity of design and the minimum number of components required.

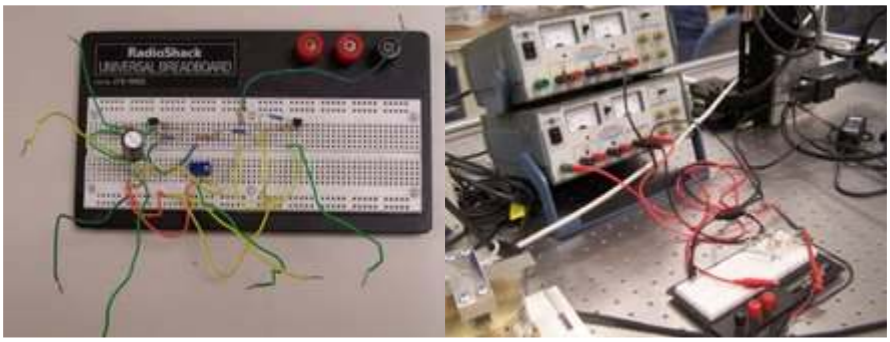

Figure 4.6: (a) Preamplifier circuit constructed on a bread board. (b) Preamplifier testing station with a bias supply voltage and power supply.

dSPACE® R & D Controller Board

The version of dSPACE® R & D Controller board used is DS1103®. The controller board can be interfaced and software programmed using Simulink® Software [75]. The interfacing with the Simulink® software provides ease of operation by allowing graphical manipulation of I/O blocks. dSPACE® R&D controller board helps in the hardware implementation of the control algorithms developed by the Simulink® software [75]. The dSPACE® provides a range of interfaces which include 50 bit I/O channels, 36 A/D channels and 8 D/A channels. These interfaces allow simultaneous acquisition of data

from various actuators and sensors. An onboard DSP controller unit TMS 320F20 ® facilitates the fast processing of the acquired data.

The DS-1103® is designed for rapid control prototyping and this characteristic feature widens its area of applications to [75]:

1) Active Vibration Control
2) Developing position control for motors like DC Servo Motor, DC Stepper Motor and Induction Motors.
3) Robotics

Figure 4.7: dSPACE® DS -1103 Controller Board Connected to the PZT Servo Controller [70].

Interfacing of C-809 Motion I/O® with d-SPACE® DS-1103 R & D Controller Board

The Pin assignment was done as shown:

Table 4.1 Matching of the pins between the C-809 Motion I/O® and d-SPACE® side

C-809 I/O Motion Side®			d-SPACE® Side
Functions	Pin No:	Pin No:	Functions
1. Axis 1 Encoder Phase A	36	CP-19-2	PHIO (1)
2. Axis 1 Encoder Phase B	37	CP-19-4	PHI90(1)
3. Axis 1 Encoder Index	38	CP-19-6	IDX(1)
4. Digital Ground	2	CP-19-10	GND
5. Axis 2 Encoder Phase A	42	CP-20-2	PHIO(2)
6. Axis 2 Encoder Phase B	43	CP-20-4	PHI90(2)
7. Axis 2 Encoder Index	44	CP-20-6	IDX(2)
8. Digital Ground	8	CP-20-10	GND
9. Axis1 Home Switch	4	CP-17-20	IO0
10. Axis 1 Forward limit switch	39	CP-17-2	IO1
11. Axis 1 Reverse Limit Switch	40	CP-17-21	IO2
12. Axis 2 Home Switch	10	CP-17-3	IO3
13. Axis 2 Forward Limit Switch	45	CP-17-23	IO4
14. Axis 2 Reverse Limit Switch	46	CP-17-5	IO5
15. Axis 1 Inhibit	6	CP-17-24	IO6
16. Axis 1 Trigger	5	CP-17-6	IO7

17. Axis 2 Inhibit	12	CP-17-26	IO8
18. Axis 2 Trigger	11	CP-17-8	IO9
19.Axis 1 Breakpoint	26	CP-17-27	IO10
20.Axis 2 Breakpoint	60	CP-17-9	IO11
21.Analog I/P 1	32	CP-1	Analog to Digital Converter
22.Analog I/P 2	66	CP-2	Analog to Digital Converter
23.Analog O/P1	29	CP-9	Digital to Analog Converter
24.Analog O/P 3	63	CP-10	Digital to Analog Converter
25.Digital Ground	2	CP-17-1	GND
26. Host +5 V	59	CP-17-36	V *cc*

A Short Description of the Interfacing

The pins from serial numbers 1 to 20 are digital in nature. This fact necessitated using the Digital I/O port of the d-SPACE® for interfacing. The C-809 Motion I/O® was custom made to work with National Instruments® I/O card, so this aspect prompted to utilize the Digital I/O pins of the d-SPACE®. The first step was to tap all the digital pins on the C-809 I/O Motion Side. Accordingly the first 20 pins were selected for interfacing and tapping the digital signals for running the micro-positioner. For pins corresponding to serial numbers 21 to 24 the nature of signals being analog prompted us to utilize the A/D and D/A ports of the d-SPACE®. At the end digital Ground and V_{CC} pins were connected for completing the interfacing process. In the beginning it was assumed that the pins breakpoint and the trigger will be required for running the micro-positioner. But later

after few preliminary level experiments it was found that the encoder phase A and B pins and Encoder index pins corresponding to each axis along with Forward, Reverse and Home Limit Switches were necessary for running each axis of the micro-positioner. Axis Inhibit pins had to be tied high i.e. a non- zero quantity of the voltage has to be supplied to the inhibit pin in order to make it run. An Analog Voltage supply is also supplied in order to vary the speed of rotation of the DC Servo Micro motor. For this purpose pin with serial number 26 was utilized. Initially the tying of the Inhibit pin with a non-zero voltage and varying of the speed of rotation of the DC Servo motor using the V_{cc} pin was done manually. Hence, the digital pins along with the analog pins were utilized in order to make the micro-positioner to run with a third party drive which is d-SPACE® in this case. But later a custom made cable was built which had a National Instruments® Cable bought from NI® for the C-809 I/O Motion® Side and the other end was a 37-pin d-Sub connector pin for the d-SPACE® side. Successful completion using this cable facilitated in establishing as well as acquiring signals pertaining to the encoder using software called "Control Desk®" easier and eliminated manual control.

Software

Software here satisfies two purposes: Automatic control of the micro positioner and the STM as a whole; Secondly processing of the image captured by STM. For the automatic control of the micro positioner Control desk ® is used for the front end and Simulink® is used for the back end. Various types of commercial softwares are available like the SPIP® (Scanning Probe Image Processor), Deconvolution Software®, GXSM® for scanning and processing of the image obtained from a STM. But for the preliminary level

experiments Matlab® has been concluded to be sufficient for the image processing of the data obtained from the air STM [76].

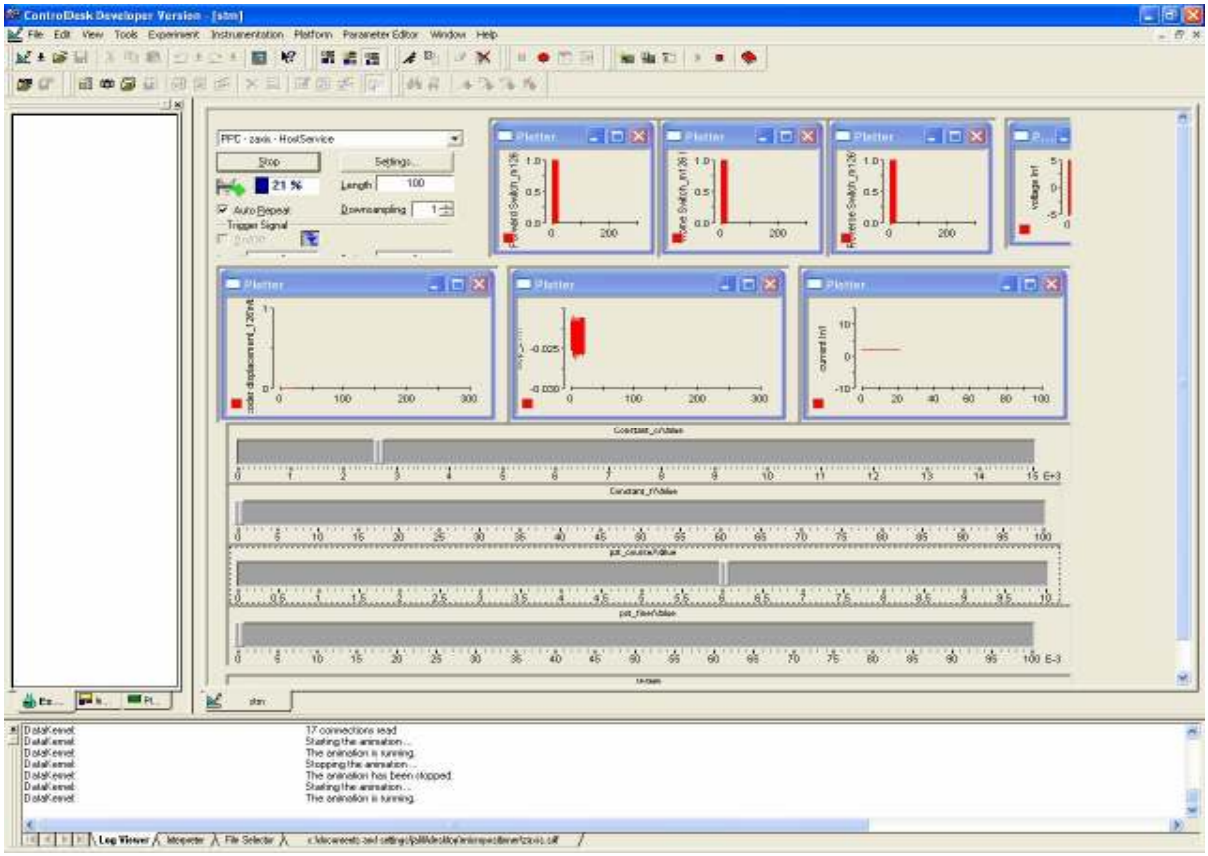

Figure 4.8: A picture highlighting the Control desk environment as the front end which is used to develop the control algorithms for the STM.

Optical System

The control of STM requires coordination of both the coarse positioner as well as the fine positioner in order to make the tip reach the optimum distance near the sample which is fixed. In the first stage the DC Servo Motor is run by adjusting the coarse positioner up

to a certain point and after that the nanopositioner is activated in order to make the tip reach an optimum distance near the sample. The second stage of control involving the nano positioner as mentioned before is in the order of nano meters. So for a precise control we need a camera or an optical system that tracks this nano meter level motion. A Pulnix® camera with a 0.67X adapter satisfies this purpose. The camera also comes with an Accupixel® Control Software that helps in simultaneous online imaging of the objects captured by the camera.

Experimental Procedure

The experimental procedure that has been described in the following lines is for the operation of a STM in the constant current mode. The entire sub system is activated by interfacing all the components. Initially the coarse positioner is run for several micrometers up to a certain point and once with the help of the micro positioner, the tip is brought within the capture range of the camera, the nano-stager (in the Z direction) is activated. At this stage the nano stager is carefully run in order to find the optimum distance between the tip and the sample. At an optimum distance the current begins to flow between the tip and the sample. Wires are soldered to the metallic part of the tip and to the stainless steel body of the cylinder (Sample Holder). Depending upon the magnitude of the current output from the preamplifier, the z height of the nano-stager is adjusted. Once the optimum distance has been established the current between the tip and the sample starts flowing. And this generation of current is based on the quantum mechanical phenomenon of matter, the theoretical aspect of which has been discussed in chapter 4. This current is amplified using a preamplifier which provides the feedback

signal for controlling the z height of the micro positioner. The optimum distance in the initial stages is reached by trial and error, as it depends on the type of the sample to be imaged and the magnitude of the bias voltage that is applied between the tip and the sample After an observable magnitude of tunneling current has been sensed through one of the D/A channels of the d-SPACE® R & D controller board, the movement of the Z stager is stopped. The X and Y stagers of the nano-stager are activated depending upon the requirement in order to complete the scanning of the sample placed on the sample holder. Various numerical values would be obtained corresponding to the X, Y and Z directions using which surface profile of the sample is generated with the help of Matlab®.

Following precautions need to be taken before beginning the imaging process:

a) The tip and the sample holder need to be cleaned initially using acetone and then using ethanol in order to remove the sweat and the oils that could have accumulated during the handling of the sample and the tip holder. It is necessary to clean the oils and the fluids as they contribute to the conduction losses during the passage of the nano level current.
b) If the tip is to be cut from a wire then it should be etched in an angular way so that the edge of the tip contains only a single atom thus facilitating the tunneling process when the tip is brought in close proximity to the sample.
c) The cut tip also needs to be handled by using a tweezer so that they are not exposed to the naked hands.
d) Gloves also should be worn while handling the components of STM head.

Based on the design criteria outlined by Dieter.W.Pohl, it has been thought to be essential to cover the entire experimental set up with a glass enclosure in order to prevent noise and external vibrations during the imaging process.

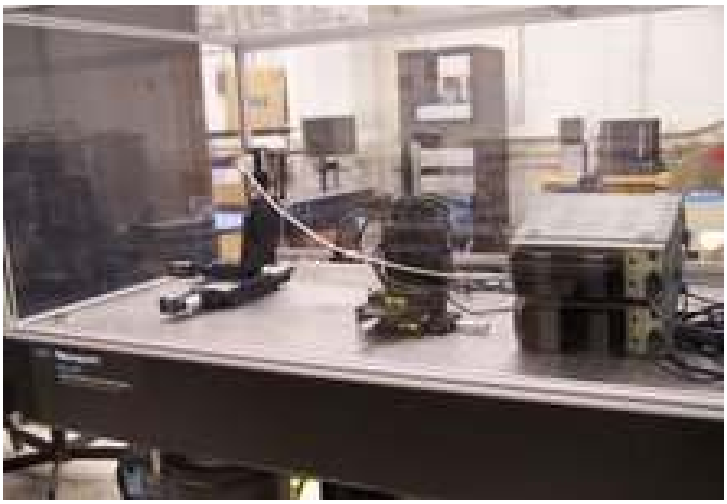

Figure 4.8: Back view of the experimental set up mounted on an optical bench and enclosed inside a glass case.

Details of designs of STM apparatus have been provided in the appendix

Chapter Summary

Various sub systems constituting the Scanning Tunneling Microscope test bed have been described. The process of interfacing of the micro-positioner with the d-SPACE® R & D controller board along with the pin assignment has been discussed. The other apparatus like STM Electronics, optical subsystem, nano stager etc and their operation have been described. Chapter 5 discusses about the results.

CHAPTER 5

RESULTS AND DISCUSSIONS

As mentioned in Chapter 2, the tunneling current acts as the feedback signal in the control of the height of the Z stager in the constant current working mode. The plot shown in Figure 5.1 shows the ouput voltage of preamplifier circuit when the tunneling gap distance in the circuit is varied.

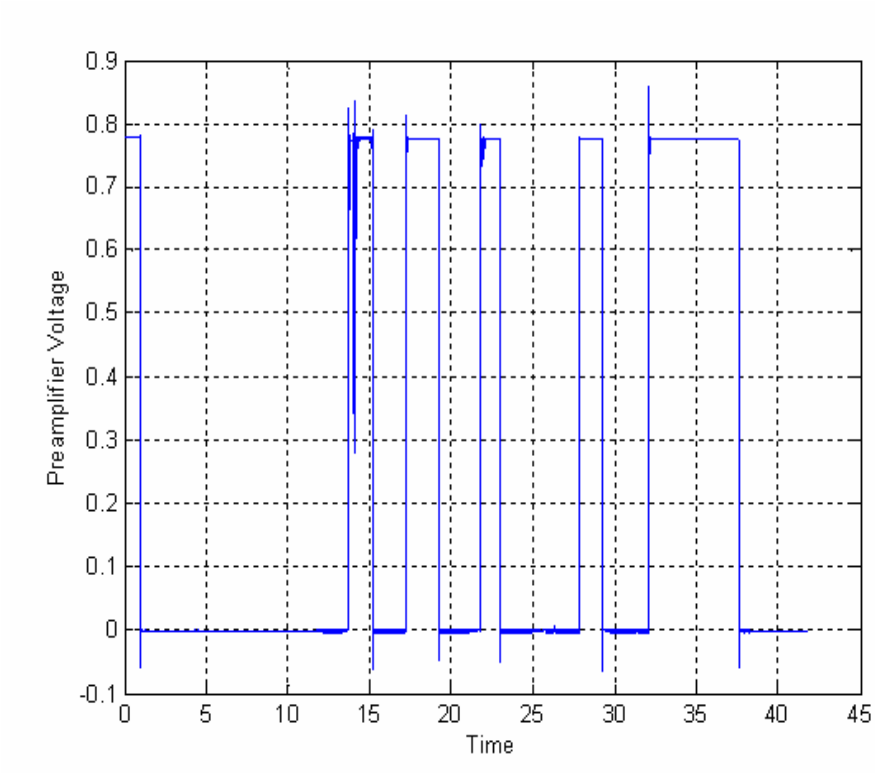

Figure 5.1(a): Plot of the preamplifier voltage in volts with respect to time in seconds

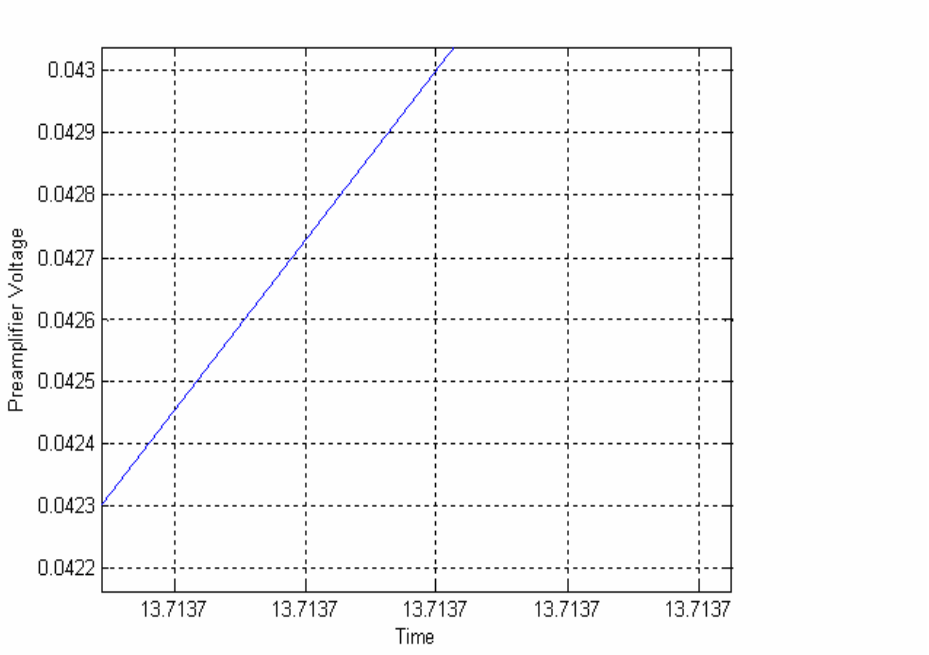

Figure 5.1 (b) Zoomed plot of variation of preamplifier voltage with time in seconds

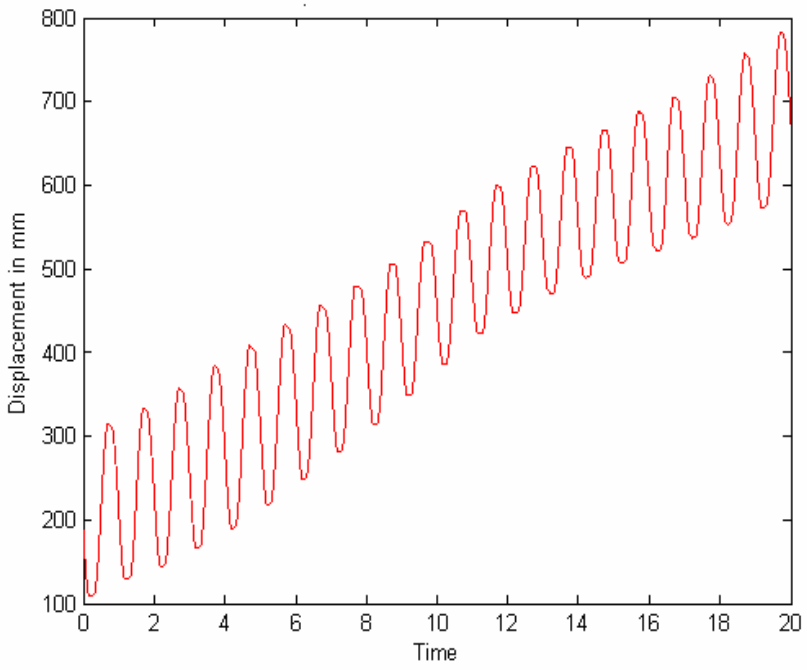

Figure 5.2 Plot of displacement of micropositioner for a sinusoidal input

Displacement of the micropositoner is a function of this tunneling current. The plot of Figure 5.2 indicates the displacement of the micropositioner for a sinusoidal input. From Figure 5.2, we can observe that for a sinusoidal input the output must go spiraling downwards but on the contrary it spirals upwards due to the position of the encoder and the displacement of the DC micro-motor from the Home switch towards the Forward limit switch.

The preamplifier circuit given in [72] is shown in Figure 5.3:

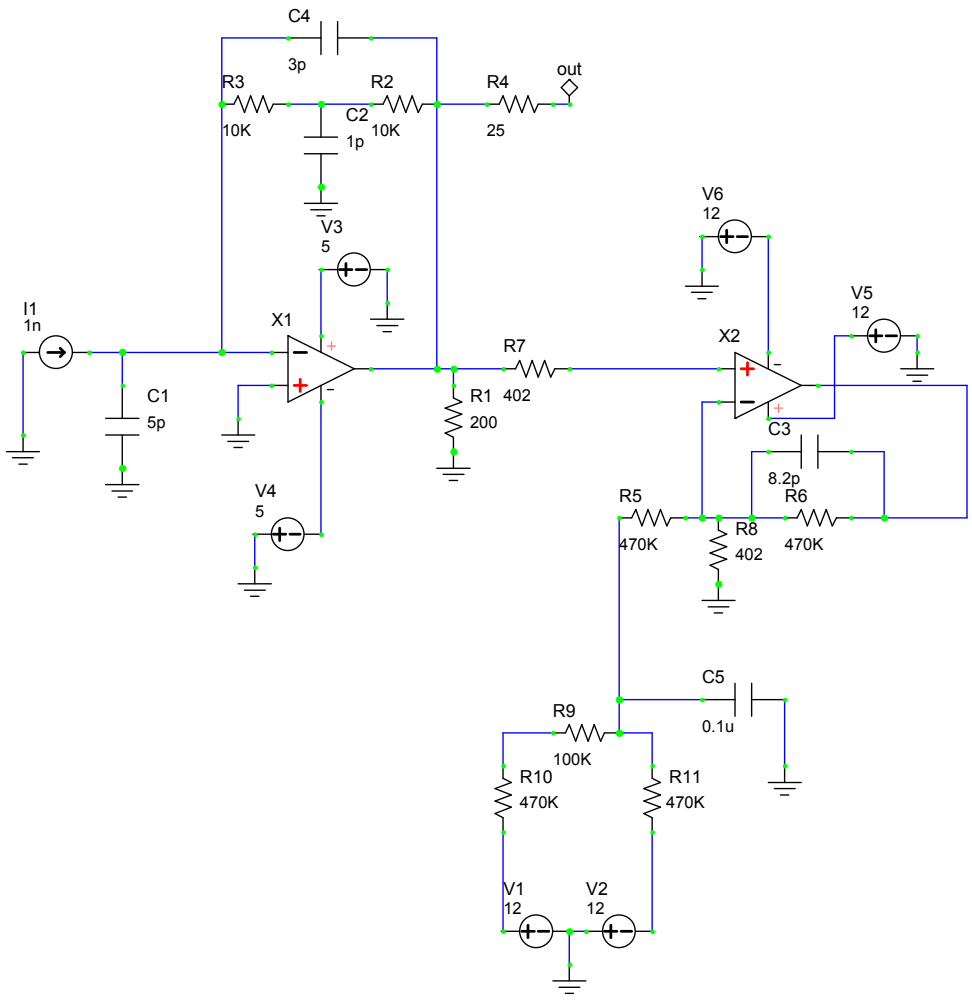

Figure 5.3: A circuit diagram showing a pre-amplifier used in STM [72].

PSPICE® was used to run basic simulations for the circuit diagram given in Fig 5.3. The simulations of the circuit are as shown in Figure 5.4 and Figure 5.5:

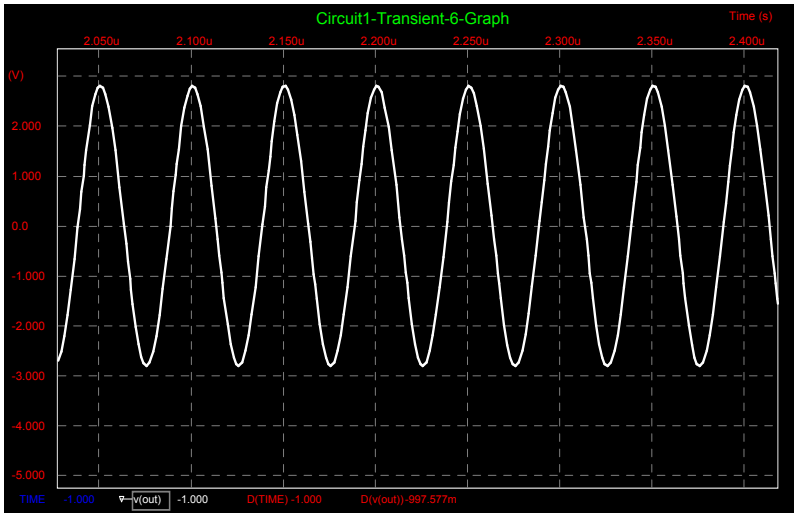

Figure 5.4: The input conditions for the preamplifier were 1 nano ampere (current source assumption), 20 MHz, 1 μV peak to peak

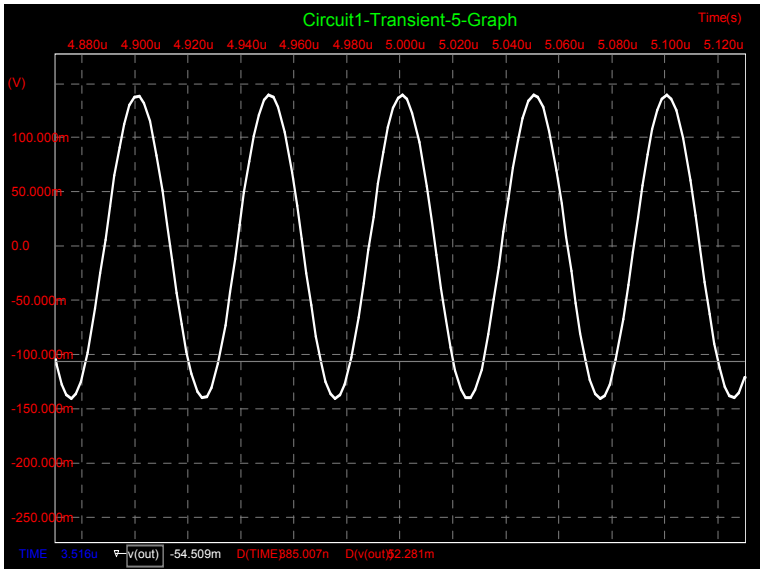

Figure 5.5: The input conditions for the preamplifier were 1 nano ampere (current source assumption), 20 MHz, 1 mV peak to peak

CHAPTER 6

CONCLUSIONS

In the above thesis work an attempt has been made to build and fabricate an in house STM. To understand the system better, an analysis was done on the design of SPM (in general) based on the past literature. The developments that has taken place in the field of tip to sample interaction have also been discussed, which facilitate in the interpretation of the physics of the phenomenon between the tip and the sample. This was followed up by a practical effort to build an in house STM by interfacing various subsystems. The initial task was to automate the control of the micro positioner and establish a software control of the micro positioner with Simulink® as the back end and the Control desk® as the front end. There were other auxiliary apparatus that were designed for the STM like STM electronics, STM head (STM tip holder and Sample holder) to complete the test bed. Many preamplifier circuits were tested for their effectiveness. A preamplifier with minimum number of passive components was constructed in order to amplify the voltage and provide the feedback signal. This feedback signal will be utilized to control the height of the micro-positioner in the Z direction. An optical sub system in the form of a high resolution camera from Pulnix® has been interfaced to facilitate a dual stage control. The entire experimental set up has been enclosed in a glass case. Though, under the present conditions nano level images have not been attained but, it can be confidently stated that with some modifications to the present fabricated experimental set up (which might typically involve replacement of the current dSPACE® R & D controller board

with a higher resolution data acquisition board) and some more attempts, acquisition of nano level images is feasible.

Future Work

This project work can be rightly described as a “fertile ground “for further research. The future work would involve the design and implementation of various types of non linear controllers for the coarse positioner as well as for the STM as a whole. The effectiveness of the controllers would be a direct measure of the resolution of the nano level images obtained using the STM. The coarse positioner that has been fabricated has non linearties like backlash and friction which can be included in the design of the non linear controllers. Though, at present the acquisition of nano level images has not been carried out due to the hardware constraints (like resolution) pertaining to the data acquisition board. But in the future a higher resolution data acquisition board like Data physics® can solve the problem of acquiring images. The camera that is used for zooming in during the fine positioning of the tip to sample interaction can be used as a tool in developing controllers based on visual feedback. Better image processing algorithms can also be implemented in order to provide better graphics user interface for the acquisition of data and visualization of the fine as well as coarse positioner. The preamplifier which has now been constructed on a bread board and placed near the STM at a distance can be made more sophisticated by soldering it on a Printed circuit board and placing it near the STM head, which will shorten the length of the wire going into the bread board and hence reduce considerably the electrical noise associated with it. An enclosure typically made of steel or brass can also be provided to cover the STM preamplifier in order to make it

less sensitive to the vibrations which might affect the resolution of the images to be obtained. The fabrication can also be made more “in house” or indigenous by creating a tip manufacturing module. This module may typically include a dessicator to facilitate cleaning the cylindrical sample holder and tip holder. The advantage of possessing such a module near the test bed itself will facilitate un- interrupted supply of tips during the imaging process, because there is a high probability of occurrence of tip to sample crash. Future work may also involve nano indentation and nano manipulation using the present experimental set up as a base and with additional improvised instrumentation.

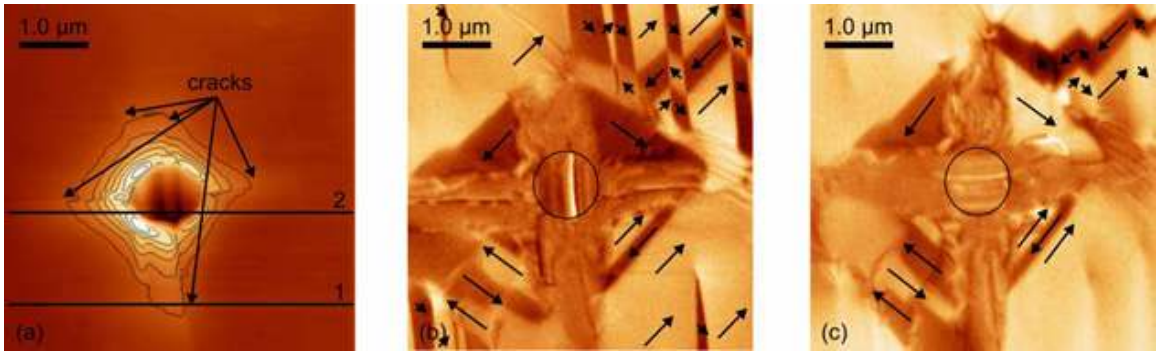

Figure 6.1: Topography image of a surface in which nano indentation has been done. [77].

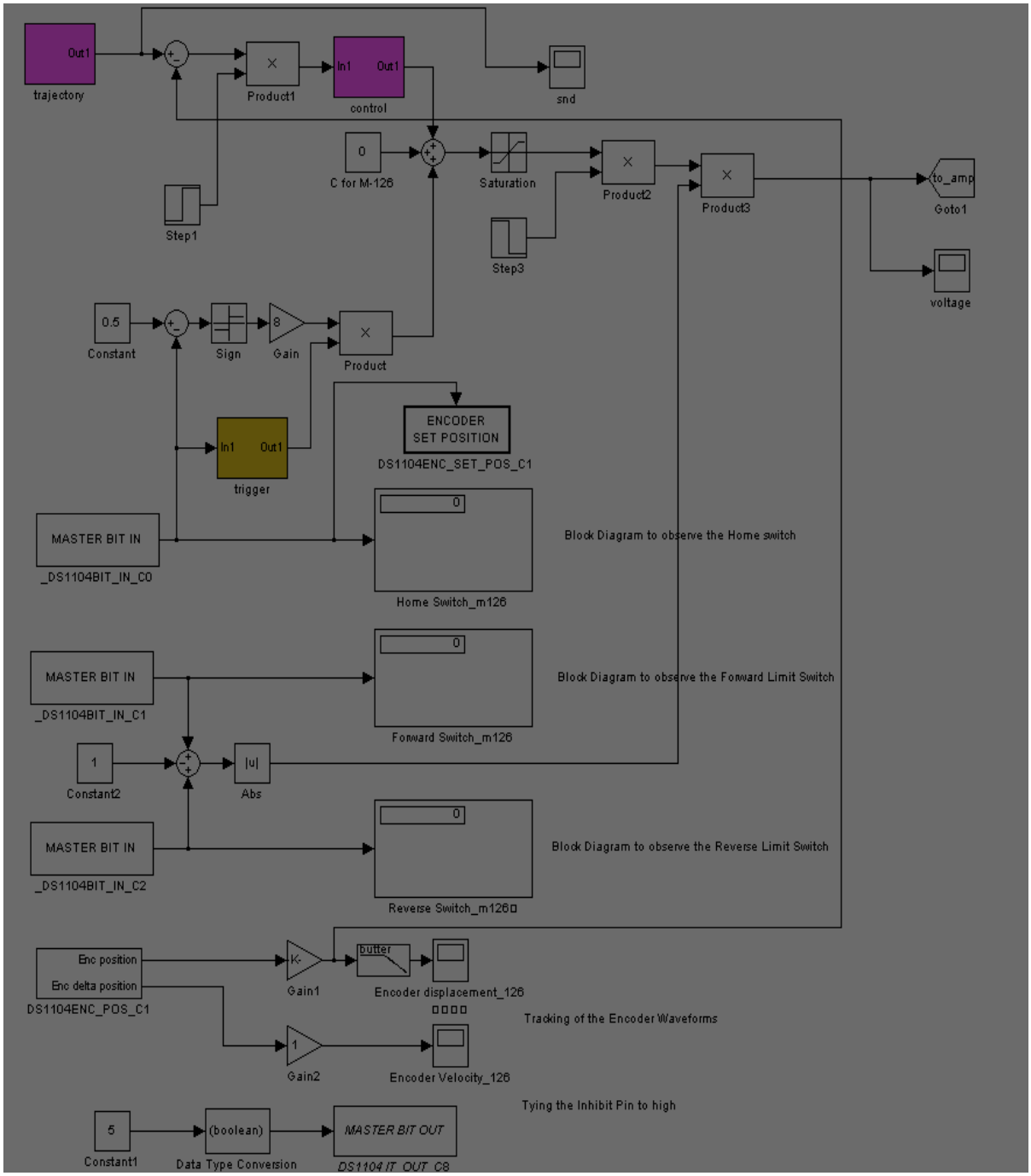

Figure 6.2: A layout of the control algorithm that is being developed to control the scanning process of the air STM that has been built with Simulink ® software as the backend.

APPENDICES

Appendix A

Design Diagrams of STM Head

The design of the tip holder is as shown in Figure A.1, Figure A.2 and Figure A.3:

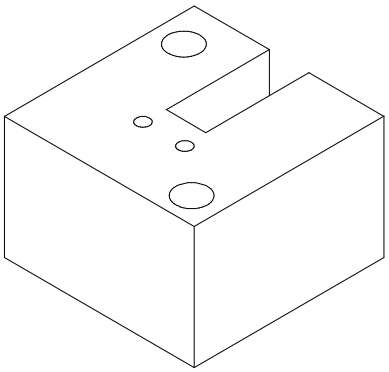

Figure A.1: A Schematic of a fixture for holding the two legs of the tip holder.

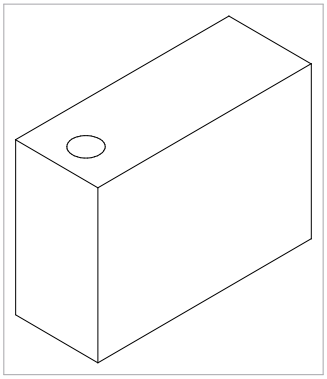

Figure A.2: A Schematic of a fixture for holding the conducting leg of the tip holder.

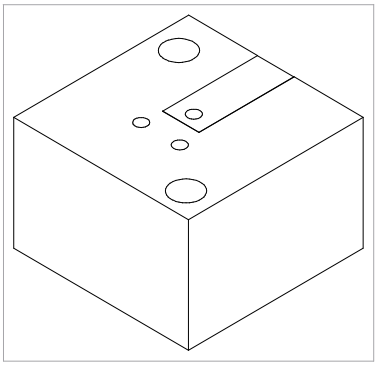

Figure A.3: A Schematic of a fixture that has been formed by combining both the fixtures shown in Figure A.1 and Figure A.2

The tip holder fixture was designed keeping in perspective that the tip holder used in the experiment was specifically manufactured by Omicron® technologies and was designed to be used in Vacuum

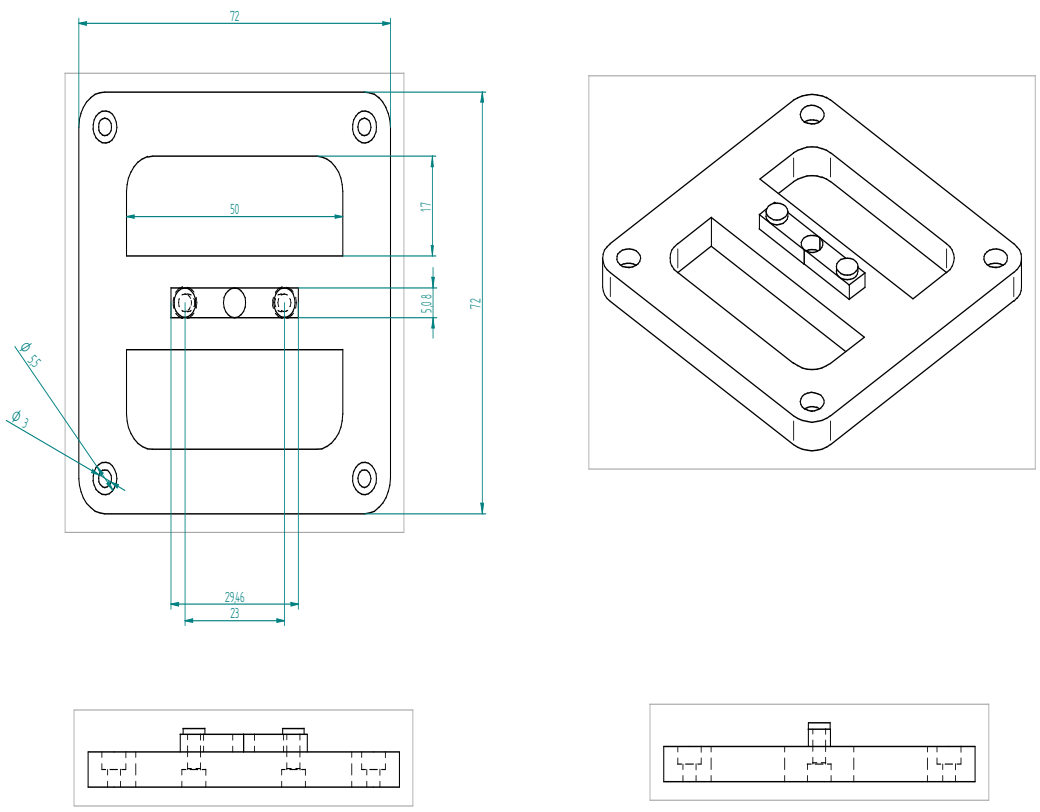

Figure A.4: Design of a fixture for holding the cylindrical sample holder upon the X and Y axes Nanostager bought from PI®

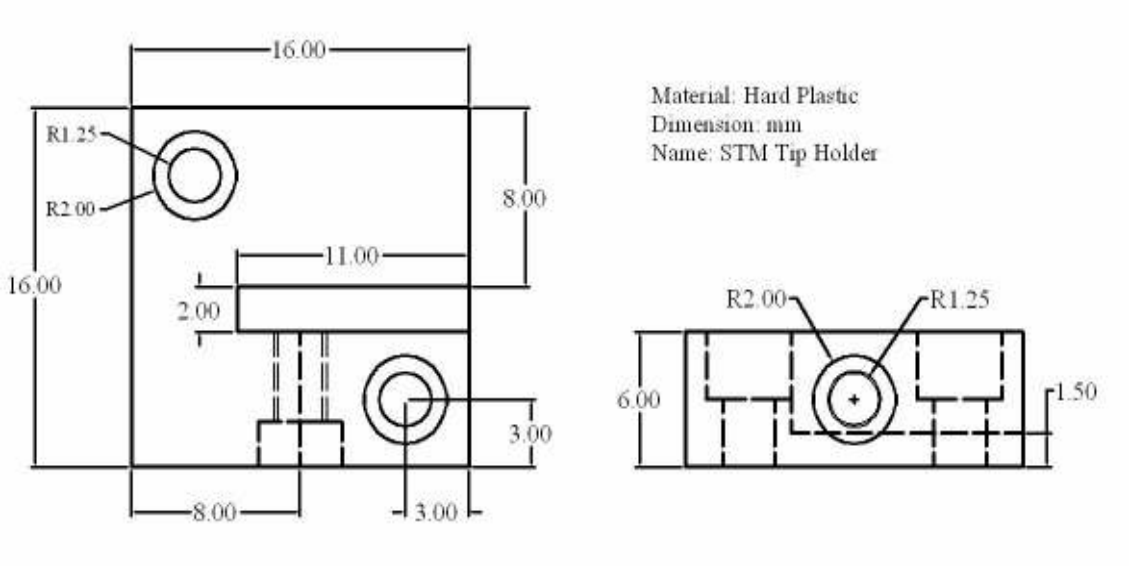

Figure A.5: Design of the fixture to hold the tip using a screw which was mounted on the P-753 Nano automation® stager

Figure A.6: The sample holder shown below was designed and manufactured in two steps:

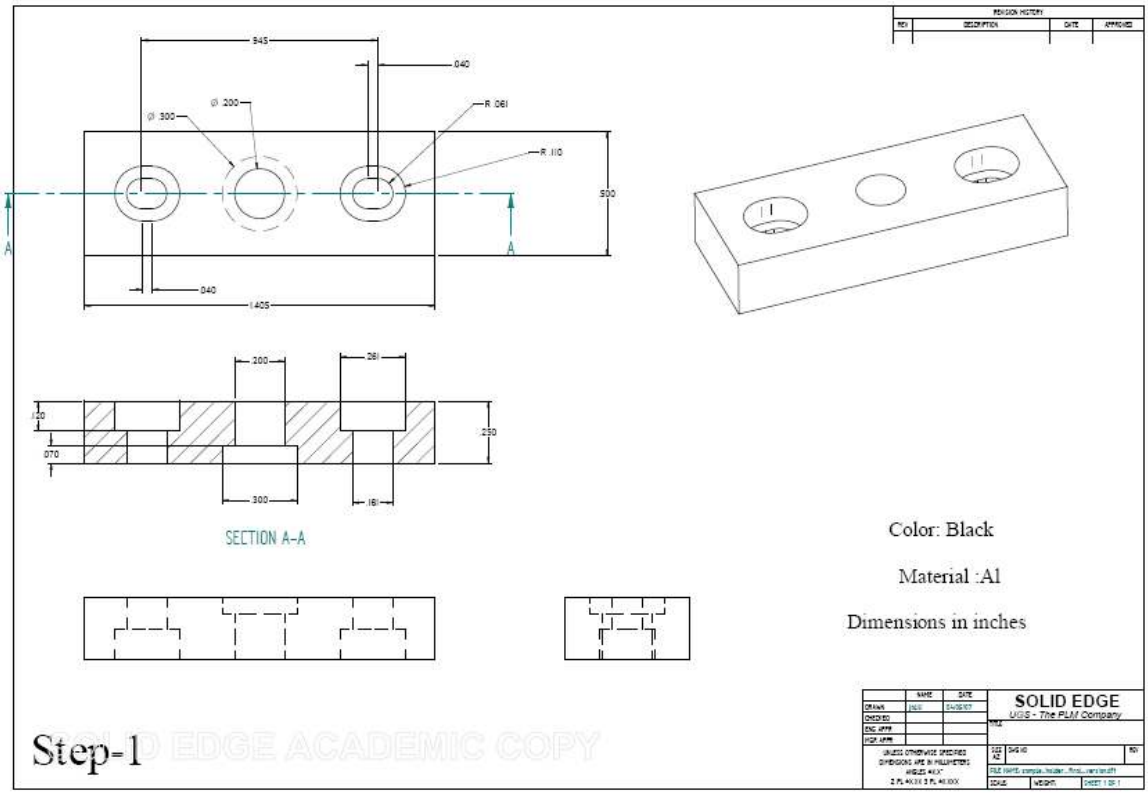

Step 1: The sample was designed and manufactured as a single piece as shown above.

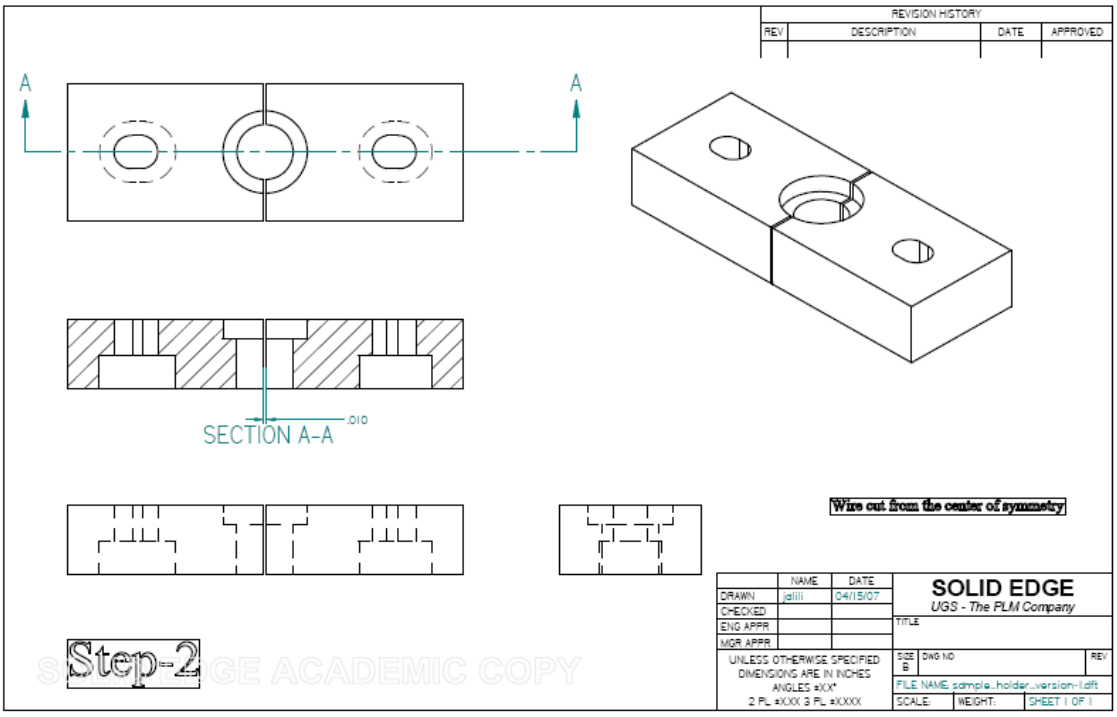

Step 2: The whole piece was then wire cut exactly at the center of symmetry

Appendix B

Images related to STM Preamplifier

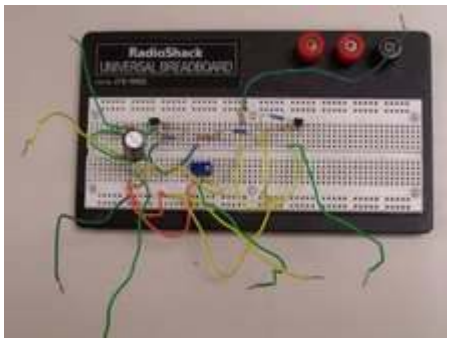

Figure B.1: Image of a preamplifier that was constructed with a provision to change the gain of the circuit using a potentiometer

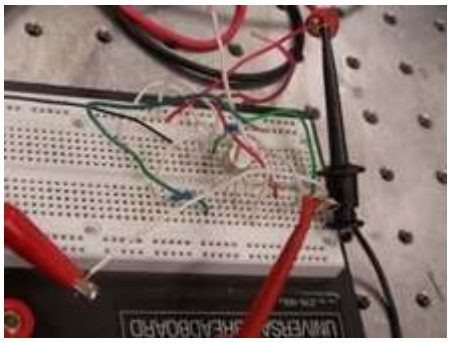

Figure B.2: Image of a preamplifier [74] on a bread board that is being used in the STM test Bed

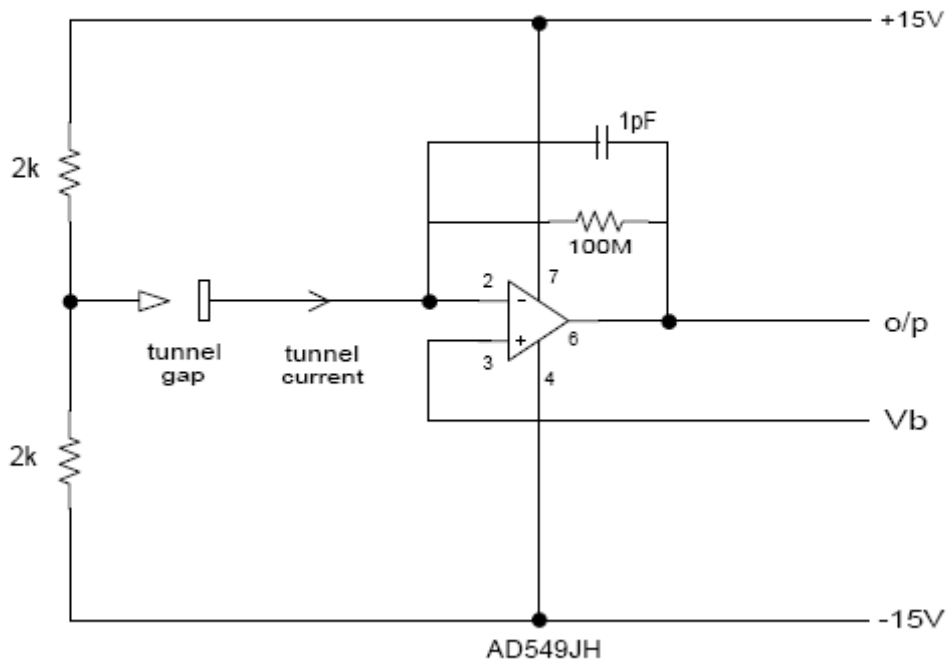

Figure B.3: Circuit diagram of the preamplifier that has been constructed [74]

Appendix C

List of Equipments

Micro-positioner

The micro positioners bought from Physik Instrumente® are "compact closed loop DC motor with a shaft mounted high resolution encoder and a precision gear head providing 0.1µm minimum incremental motion" [78].

In order to ensure protection of the equipment the stages are provided with non-contacting, Hall Effect limit (TTL drivers) and direction sensing switches (like Forward, Reverse and Home limit switches) which are placed throughout the travel range of the stager. These switches are responsible for controlling the over-travel of the stager. They also prevent the stager from coming to a hard stop. As mentioned earlier, the Hall Effect switches in the stager provide TTL signal as to whether the stage is to the negative or the positive side of the fixed point [79]. Both the M-126 DG1® and M-410 DG1® possess these Hall Effect switches. The travel range of the M-410 DG 1® is 100 mm and its maximum velocity is 1.5 mm/ sec. The travel range of the M-126 DG1® is 25 mm and the maximum velocity is 1.5mm/sec.

Figure C.1: A picture of the M-126 DG1 which belongs to the same genre of M-126 DG1 stagers [78]

Figure C.2: A picture of the M-410® series of translational stagers [79].

Both these stagers are driven by an armature controlled DC servo motor manufactured by Faulhaber® the output power of which is 1.75 watts. There are also variants of the same

genre of stagers which are driven by stepper motors but they are not chosen as servo motors use a feedback from the motor to help the motor get to a desired state. [82]

The detailed specifications about the motor constants are found in [86].

Nano-positioner [83]

The Nano positioner similar to the micro-positioner is capable of movement in all the three directions viz X, Y and Z. The P-753® Nano Automation stage actuator from PI is the one that has been used as the Nano-positioner. The characteristic features of the Nano-positioner are its scanning range of up to 38 μm and very fast settling time [81]. The stage actuators are also extremely fast and compact devices. They can be used as both linear actuators as well as translation stages. The sub-nanometer resolution of around 0.05 nm is attributed to the capacitive feedback sensor incorporated in the Nano Automation stage actuator. The above mentioned characteristic features make it ideally suited for Precise Trajectory Control for use in applications like Scanning Microscopy, Scanning interferometry, Micromanipulation etc.

Figure C.3: LISA® Nano Automation Stage actuators [81]

A single module, XY Piezo flexure Nano-positioner and Scanner

The P-733® single module, XY Piezo flexure Nanopositioner and Scanner stager provides the X and Y axes movement. The scanning range provided by them is around 100 X 100 μm and similar, to P-753® Nano Automation stage actuator the sub-nanometer and nanometer level accuracy is obtained owing to the capacitive feedback sensors. The Nano stager works on the principle of Parallel Kinematics, which provides the Nano-positioner with the advantage of elimination of cables [83]. The elimination of cables helps in providing better accuracy and resolution at the sub nanometer level as this also helps in reducing friction. The additional advantages being increased responsiveness and repeatability [83]. The field of applications is the same as that mentioned for P-753® Nano Automation Stage Actuator.

Figure C.4: P-733® Flexure Nano-positioner [81]

Power Supply Units

Figure C.5: A picture of the CPS 250 power supply units from TEKTRONIX® [84]

Two CPS 250 Power Supply Units (each with one fixed 5V, 2A and two variable 0 to 20 V and 0.5 A power supplies) from Tektronix® were used for supplying bias voltage and power supply to the AD 549 JH op amp in the preamplifier.

REFERENCES

[1] Smith, R., James, 1997, "An Overview to Scanning Probe Microscopy*", Educ. Chem*, **Vol. No: 34,** 4, P.107-111

[2] Bai, C., 2000, "*Scanning Tunneling Microscopy and its Applications*", Springer Verlag, New York.

[3] URL: http://www.zyvex.com/nanotech/feynman.html- A website dealing with the Speech delivered by Dr. Richard Feynman on December 29th 1959. Cited 04/25/2007

[4] URL:http://www.lbl.gov/LBL-Programs/TEAM/: A website dealing with the National Center for Electron Microscopy: Cited 04/15/2007

[5] Vida-Simiti, I., Jumate, N., Chicinas, I., Batin, G., 2004, "Applications of Scanning Electron Microscopy in Nanotechnology and Nanoscience"*, Rom. Journ .Phy. ,* **Vol No: 49**, 9-10, P.955-965, Bucharest Meeting of the American Physical Society at the California Institute of Technology.

[6] Binnig, G and Rohrer, H., 1984, *in "*Trends in Physics"*,* (editors: J.Janta and J. Pantoflicek, *European Physical Society*, P.38-46

[7] Dovek, M. M., Heben, M. J., Lewis, N.S., Penner, R.M., Quate, C.F., 1988, "Applications of Scanning Tunneling Microscopy to electrochemistry"*, American Chemical Society*, **Vol No: 378**, P.174-201

[8] Lindsay, S.M., Nagahara, L.A., Thundat, T., Knipping, U., Rill, R.L., Drake, Prater, C.B., Weisenhorn, A.L., Gould, S.A.C., and Hansma, P.K., 1989, "STM and AFM Images of Nucleosome DNA under water", *Journal of Biomolecular structure and Dynamics*, **Vol No: 7,** 2

[9] Liu, H.Y., Fan, F.F., Lin, C.W., and Bard, A.J., 1986, *American Chemical Society*, **Vol No: 108**, P. 3838-3839

[10] Sonnenfeld, R., and Hansma, P.K., 1986, *Science,* **Vol No**: **232**, P.211-213

[11] Drake, B., Prater, C. B., Weisenhorn, A.L., Gould, S.A.C., and Hansma, P.K., 1989, *Science,* **Vol No**: **243**, P.1586-1589

[12] Thundat, T., Nagahara, L.A., Oden, P., and Lindsay, S.M., 1989, "Direct Observation of Bioelectrochemical Processes by STM", *J.Vac.Sci.Technol,* **Vol No: A,** 8**,** 1, P.645-648

[13] Girard, J.C., Gauthier, S., Rousset, S., and Kelin. J., 1993, "Investigations of the Morphology of copper surfaces by scanning tunneling spectroscopy", *Microsc.Micoranal. Microstruct,* **Vol No**: **4,** P.489-499

[14] Bonnell, A., Dawn," *Scanning Probe Microscopy and Spectroscopy Theory, Applications and techniques*", John Wiley & Sons, New York, 2001

[15] Tao, N. J., Li, C. Z., He, X., 2000, "Scanning Tunneling Microscopy Applications in Electrochemistry- beyond imaging", *Journal of Electroanalytical Chemistry*, **Vol No: 492,** P.81-93

[16] Website: www.mrs.org/publications/bulletin A website containing a bulletin board That deals with the applications of Scanning Tunneling Microscopy in Material Cited 05/10/2007

[17] Heinz Reider –Karl, Meyer Gerhard, Wai Hla- Saw, Moresco Fracesca, Brown, F., Kai, Morgenstern Karina, Repp Jascha, Foelsch Stefan and Bartels Ludwig, 2004, "The Scanning Tunneling Microscope as an operative tool: doing Physics and chemistry with single atoms and molecules", *Phil.Trans.R.Soc.Lond* A, **Vol No: 362**, P.1207- 1216

[18] Booklet on "Thermo Microscopes", highlighting the SPM techniques.

[19] Ressel, B., *Practical Aspects of Scanning Probe Microscopy,* ICS Training Course on Experimental Methods in Nanophotonics, Trieste (Italy), 21-25 February, 2005. Cited: 09/04/2007

[20] Hansma, G., Helen and Jan, .H, Hoh, 1994, "Biomolecular Imaging with the atomic Force microscope", *Annu. Rev. Biophys. Biomol. Struct.* , **Vol No: 23,** P.115-39

[21] Putman, C.A., van der Werf, K.O., de Grooth, B.G., van Hulst, N.F., Greve, J., 1992. "New imaging mode in atomic force microscopy based on the error signal", *Proc. SPIE Int. Soc. Opt. Eng*, **Vol No: 16389**, P.198-204.

[22] Jalili, N., and Laxminarayana, K., 2004, "A review of atomic force microscopy Imaging systems: application to molecular metrology and biological sciences", *Mechatronics,* **Vol No: 14,** P.907-945.

[23] Wright, L., Tanya, Master's thesis, May 2005, titled "Fabrication and testing of Heated Atomic Force Microscope Cantilevers", presented to Department of Mechanical Engineering, Georgia Institute of Technology

[24] URL: http://vpd.ms.northwestern.edu/teaching/AFM_MSc_190_lab.pdf: A PDF File dealing with Atomic Force Microscopy published by North Western University Cited: 05/10/2006

[25] Hofer, A., Werner, Foster, S. Adam, Shluger, L., Alexander, Oct 2000," Theories of Scanning Probe Microscopes at the atomic scale"*, Review of Modern Physics*, **Vol No: 75**.

[26] URL: http://www.webpages.uidaho.edu/~aston/AFMShortCourse2001.docl : Website dealing with a Short Course on "Surface and Colloid Science" by Dr. Eric Aston on July 9-13, 2001, University of Washington, Department of Chemical Engineering, Seattle, Washington, Cited: 04/15/2007

[27] Rugar, D., Mamlin, H.J., Guethner, P., Lambert, S.E., Stern, J.E., McFadyen, I., and Yogi, T., August 1 1990, "Magnetic force microscopy: General principles and Application to longitudinal recording media"*, J.App.Phys,* **Vol No**: **68,** (3)

[28] Martin, Y. and Wickramasinghe, H.K., 18 May 1987, "Magnetic imaging by "force Microscopy" with 1000 Å*", Appl. Phys. Lett*, 50, **Vol No**: **20**.

[29] Williams, C.C., 1999, *Annual Review Material Science,* **Vol No*: 29***, 471

[30] Barrett, R.C., Quate, C.F.*,* 1990, *J.Vac.Sci. Technol,* **Vol No**: **A8**, 400

[31] Kopanski, J.J., Marchiando, J.F., and Lowney, J.R., Jan/Feb 1996," Scanning Capacitance microscopy measurements and modeling: Progress towards dopant Profiling of Silicon"*, J. Vac. Sci. Technol*., B, **Vol No: 14,** 1

[32] Barrett, R.C., and Quate, C.F., Jan/Feb 1990,"Imaging polished sapphire with Atomic Force microscopy"*, J. Vac. Sci. Technol*., **Vol No: A8,** 1

[33] Majumdar, A., 1999," Scanning Thermal Microscopy", *Annu.Rev.Mater.Sci*., **Vol No: 29**, P.505-85

[34] Pylkki, J., Russell, Moyer J., Patrick, and West, E., Paul, 1994, "Scanning near Field Optical Microscopy and Scanning Thermal Microscopy", *Jpn. J. Appl. Phys*., **Vol No: 33,** P.3785-3790

[35] Williams, C.C., and Wickramasinghe, H. K., 1986: *Appl. Phys. Lett*., **Vol No: 49** 1387

[36] Majumdar, A., Carrej, J.P., Lai, J., 1993, *Appl .Phys. Lett***, Vol No: 62**, P.2501-3

[37] URL: http://www.triple-o.de/pages/application_spm.html#snom Cited: 07/12/2007

[38] Abbe, E., *Archiv. Mikros. Anat,* 1873, **Vol No: 9**, 413.

[39] URL: http://www.jpk.com/tutorial/snom_principle.htm Cited: 05/10/2007

[40] Dunn, C., Robert, "Near-field Scanning Optical Microscopy", *Chemical Reviews*, 1999, **Vol No: 99**, 10.

[41] R.Toledo-Crow, P.C.Yang, Y.Chen, and M.Vaez-Iravani, *Near-field differential Scanning optical microscope with atomic force regulation,* Appl. Phys .Lett, **Vol No: 60**, 24, 15 June 1992

[42] Cline, J.A., Barshatzky, H., and Isaacson, M., 1991, *Ultramicroscopy,* **Vol No**: **38**, 299

[43] Pohl, D.W., Fischer, U.C., and Durig, U.C., 1988, *J.Microsc.* **Vol No: 152**, 853

[44] Grober, D. R., Harris, D.T., Trautman, K. J., and Betzig, Eric, March 1994, "Design and Implementation of a low temperature near field- scanning optical Microscope", *Rev. Sci .Instrum*, **Vol No: 65**, 3.

[45] Crow, R.-Toledo, Yang, P.C., Chen, Y and Vaez-Iravani, M., 15 June 1992,"Near-field differential scanning optical microscope with atomic force regulation", *Appl. Phys. Lett*, **Vol No: 60**, 24.

[46] Betzig, E., Finn, P.L., and Weiner, J.S., 1992, *.Appl.Phys.Lett,* **Vol No: 60**, 2484.

[47] Talley, C.E., Cooksey, G.A. and Dunn, R.C., 1996, *Appl. Phys.Lett.,* **Vol No**: **69**, 3809

[48] Colinge, J. P., Colinge, C. A., 2002, "*Physics of Semiconductors Devices*", *Kluwer Academic Publishers*, Dordrecht, The Netherlands.

[49] Drakova, D., 2001," Theoretical modeling of scanning tunneling microscopy, Scanning tunneling spectroscopy and atomic force microscopy", *Reports on Progress in Physics*, **Vol No**: **64**, P.205-290.

[50] Bardeen, J., 1961, "Tunneling from a many particle point of view", *Physical Revie*w *Letters*, **Vol No: 6**, 2, P.57-61

[51] Giaever, I., 1960,"Energy gap in superconductors measured by electron tunneling", *Physical Review Letters*, **Vol No: 5**, 4, P. 147-148

[52] Wolf, E.L., 1985, "*Principles of electron tunneling spectroscopy*", *Oxford University Press,* Oxford.

[53] Albrecht, P., Ritter, K., Ruppalt, L., "The Bardeen Transfer Hamiltonian Approach To Tunneling and its Application to STM and carbon Nano tubes", A presentation On May 5, 2004 at Beckmann Institute for Advanced Science and Technology at UIUC, USA.

[54] Van de Leemput and Kempen, H. Van, 1992, "Scanning Tunneling Microscopy", *Reports on Progress in Physics*, **Vol No: 55**, P.1165-1240

[55] Koetter, E., Drakova, D., Doyen, G., 1996, "Role of the tip atom in STM and AFM: Theory of atom transfer", *Physical Review .B*, **Vol No: 53**, 24.

[56] Tersoff, J and Hamann, D.R., 1983, "Theory and application for the Scanning Tunneling Microscope", *Physical Review Letters*, **Vol No: 50**, 25.

[57]URL: http://wwwex.physik.uni-hlm.de/lehre/physikalischeelektronik/phys_elektr/node233.html Cited: 05/10/2007

[58] Sacks, W., and Noguera, C., Mar/Apr 1991, "Beyond Tersoff and Hamann: A Generalized expression for the tunneling current", *J.Vac.Sci.Technology*, B **Vol No**: **9,** 2

[59] Longini, L.R., 1997, "Introductory to Quantum Mechanics for the Solid State", *Wiley-Inter-science*, John Wiley and Sons, New York

[60] Winterrlin, J., Wiechers, J., Brune, H., Gritsch, T., Hofer, H., and Behm, R. J., 1989, *Phys.Rev.Lett*, **Vol No: 62**, 59

[61] Lippmann, B.A., 1965, "Ehrenfest's theorem and Scattering theory", *Physical Review Letters***, Vol No: 15**, 1

[62] Doyen, G and Drakova, D., Dec 1986, "Modeling Calculations for the tunneling Current from tungsten tip to a flat and stepped Nickel (100) surface" *Sur. Sci*, **Vol No: 178**, 1-3, P.375-381 (III)

[63] Hallmark, V.M., Chiang, S., Rabolt, I.F., Swalen, J.D, and Willson, R.J., 1987, *Phy. Rev.Letters*, **Vol No: 59**, 2879

[64] Doyen, G., Drakova, D., and Scheffler, M., 1993, "Green function theory of Scanning tunneling microscopy: Tunnel current and current density for clean metal Surfaces", *Physical Review B*., **Vol No: 47**, 15.

[65] Doyen, G., 1993, "Tunnel Current and generalized Ehrenfest theorem", *J. Phy: Condens. Matter*, **Vol No; 5,** P.3305-3312

[66] Kuk, Y., Silverman, P.J, Feb 1989, "Scanning tunneling microscope Instrumentation", *Review of Scientific Instruments*, **Vol No**: **60,** 2

[67] Okano, M., Kajimura, K., Wakiyama, S., Sakai, F., Mizutani, W., and Ono, M., Nov/Dec 1987 "Vibration Isolation for scanning tunneling microscopy", *Journal of Vacuum Science .Technology*, **Vol No**: **A 5,** (6)

[68] Pohl, W., Dieter, July 1986, "Some design criteria in scanning tunneling Microscopy"*, IBM. Journal Research and Development*, **Vol No: 30**, 4

[69] Park, Sang-il and Quate, C.F., Nov 1987, "Theories of the feedback and vibration Isolation systems for the scanning tunneling microscope"*, Review of Scientific Instruments*, **Vol No: 58,** 11

[70] Master's Thesis titled, "*Non-linear Modeling and Control of Piezo-electrically Driven Nano-stagers*", submitted by Mr. Saeid Bashash on Dec 2005 to the Department of Mechanical Engineering, Clemson University, South Carolina, USA

[71] URL: http://www.molec.com/Products/AFM_consumables/STM_Tips.html Cited 04/16/2007

[72] Demming, F Dickmann, K and Jersch, J., June 1998, "Wide bandwidth Tran Impedance preamplifier for Scanning Tunneling Microscope"*, Review of Scientific Instruments*, **Vol No: 69**, 6

[73] Chen, Y.P., Cox, A. J., Hagmann, M. J., and Smith, H.D.A., July 1996, "Electrometer Preamplifier for Scanning Tunneling Microscopy", *Review of Scientific Instruments*, **Vol No: 67**, 7

[74] URL: http://www.angelfire.com/electronic2/spm/Preamp.pdf. Cited 05/15/2006

[75]URL:http://www.dspaceinc.com/ww/en/inc/home/products/hw/singbord/ppcconbo.cf Cited 05/15/2006

[76]URL:http://www.mathworks.com/applications/tech_computing/description/visimage Cited 07/15/2006

[77] URL: www.tu-harburg.de/gk/research/tipsample.html **-** A website dealing with The Institute of Advanced Ceramics, Technische Universität Hamburg-Harburg Cited: 05/14/2006

[78] URL: http://www.physikinstrumente.com/en/pdf/M126_Datasheet.pdf Cited: 05/14/2006

[79] MP 42E User Manual: M-126 Series Linear Positioning Stages: Release: 2.6.0.

[80] URL http://www.physikinstrumente.com/en/primages/pi_M400_3ST_i4c_O_eps.jpg Cited: 05/14/2006

[81] User Manual from Physik Instrumente titled "Micropositioning, Nanopositioning, NanoAutomation" - Solutions for Cutting-Edge Technologies

[82] URL http://zone.ni.com/devzone/cda/tut/p/id/3656#toc3 Cited: 05/14/2007

[83] URL http://www.physikinstrumente.com/en/products/prdetail.php?sortnr=201200
Cited: 05/14/2007

[84] URL http://www.tek.com/site/ps/0,,3M-15099-INTRO_EN,00.html
Cited: 05/14/2007

[85]URL: http://www.physikinstrumente.com/en/pdf/C809_Datasheet.pdf
Cited: 05/14/2006

[86] URL: http://www.faulhaber-group.com/n41656/i120174.html: Cited 06/30/2006